CELL BIOLOGY

Noncanonical activation of GLI signaling in SOX2$^+$ cells drives medulloblastoma relapse

**Marzena Swiderska-Syn[1], Júlia Mir-Pedrol[2], Alexander Oles[1], Olga Schleuger[1], April D. Salvador[1], Sean M. Greiner[1], Cara Seward[1], Fan Yang[3], Benjamin R. Babcock[4,5], Chen Shen[6], Daniel T. Wynn[6], Avencia Sanchez-Mejias[2], Timothy R. Gershon[5], Vanesa Martin[7], Heather J. McCrea[8], Kathryn G. Lindsey[9], Carsten Krieg[9], Jezabel Rodriguez-Blanco[1,10]*

SRY (sex determining region Y)–box 2 (SOX2)–labeled cells play key roles in chemoresistance and tumor relapse; thus, it is critical to elucidate the mechanisms propagating them. Single-cell transcriptomic analyses of the most common malignant pediatric brain tumor, medulloblastoma (MB), revealed the existence of astrocytic *Sox2*$^+$ cells expressing sonic hedgehog (SHH) signaling biomarkers. Treatment with vismodegib, an SHH inhibitor that acts on Smoothened (Smo), led to increases in astrocyte-like *Sox2*$^+$ cells. Using SOX2-enriched MB cultures, we observed that SOX2$^+$ cells required SHH signaling to propagate, and unlike in the proliferative tumor bulk, the SHH pathway was activated in these cells downstream of Smo in an MYC-dependent manner. Functionally different GLI inhibitors depleted vismodegib-resistant SOX2$^+$ cells from MB tissues, reduced their ability to further engraft in vivo, and increased symptom-free survival. Our results emphasize the promise of therapies targeting GLI to deplete SOX2$^+$ cells and provide stable tumor remission.

INTRODUCTION

Brain tumors are the leading cause of cancer-related death in children, with medulloblastoma (MB) being the most common type (*1*). Genome-based classification has enabled the stratification of MB into four major distinct subgroups (*2*), each with its own molecular drivers and prognoses. Children within the sonic hedgehog (SHH) subgroup represent 30% of all MB cases. This subset of tumors is characterized by the constitutive activation of SHH signaling in the granular cell precursors (GCPs) of the cerebellum (*3*–*6*). Such activation is frequently due to mutations in the gene encoding for the SHH receptor PATCHED-1 (*PTCH1*) (*7*–*9*). Stimulation of this receptor by SHH ligand binding causes derepression of the heterotrimeric GTP-binding protein–coupled receptor Smoothened (SMO) that ultimately alters the activity, location, and stability of the three downstream glioma associated oncogene (GLI) family members: GLI1, GLI2, and GLI3 (*10*, *11*). GLI1 and GLI2 mostly function as transcriptional activators, while GLI3 mainly plays a repressor role. Noncanonical activation of SHH signaling is also frequently observed downstream of SMO and is driven by gain of oncogenic proteins or loss of tumor suppressors (*10*, *12*). To date, most of the compounds that block SHH signaling target the pivotal upstream activator component SMO (*11*). Two of these inhibitors, vismodegib and sonidegib, are undergoing clinical evaluation in patients with MB (*13*). However, rapid tumor recurrence is frequently observed in patients treated with these inhibitors (*14*–*17*).

Recent work suggests that SHH MB arises from a rare population of MB-propagating cells (MPC) expressing the transcription factor SRY (sex determining region Y)–box 2 (SOX2) (*18*, *19*). These cells actively divide during tumor initiation and hierarchically contribute to the hyperplasia of the GCPs before acquiring a stem-like quiescent transcriptional profile in full-blown tumors (*18*–*20*). The versatile nature of these cells allows them to give rise to more differentiated transit-amplifying progenies, evade therapies, and initiate tumor relapses (*18*, *19*). Accordingly, SOX2$^+$ cells have enhanced abilities to engraft in vivo and to escape various chemotherapeutics (*21*), including SMO inhibitors (*19*). Despite the central role that SOX2$^+$ cells play in treatment resistance and tumor relapse, the underlying mechanisms controlling their regulation remain largely unknown.

Because of the resistance to SMO inhibition exhibited by SOX2$^+$ MB cells (*19*), we speculated that SHH signaling would be inactive in these cells. Unexpectedly, analyses of single-cell transcriptomic [single-cell RNA sequencing (scRNA-seq)] data (*20*) revealed that SHH effectors were expressed in a *Sox2*-enriched astrocyte-like population. In this particular cell cluster, the numbers of cells expressing *Sox2* increased upon vismodegib exposure. Moreover, despite expressing biomarkers indicative of SHH signaling activation, expression of the pathway effectors *Gli1*/*Gli2* was increased by SMO inhibition in this subset of *Sox2*$^+$ cells. These data suggested that activation of SHH signaling in astrocyte-like MB cells might occur in an SMO-independent manner. Using SOX2$^+$ cell–enriched MPC cultures (*22*), we now show that the propagation of these cells is resistant to SMO inhibitors but sensitive to compounds targeting GLI family members. We further show that GLI activation in these cells is driven, at least in part, by MYC signaling. Moreover, in vivo attenuation of SHH signaling downstream of SMO in response to administration of functionally distinct GLI inhibitors (*23*–*26*) reduced the numbers of vismodegib-resistant SOX2$^+$ cells in residual tumors and impeded their propagation in naïve mouse recipients. Our current results imply that relapses observed in patients treated

[1]Darby Children's Research Institute, Department of Pediatrics, Medical University of South Carolina, Charleston, SC 29425, USA. [2]Department of Experimental and Health Sciences, Pompeu Fabra University, Barcelona 08002, Spain. [3]Molecular Oncology Program, The Dewitt Daughtry Family Department of Surgery, University of Miami, Miami, FL 33136, USA. [4]Lowance Center for Human Immunology, Department of Medicine, Emory University, Atlanta, GA 30322, USA. [5]Department of Neurology, University of North Carolina School of Medicine, Chapel Hill, NC 27599, USA. [6]Department of Oncology, Lombardi Comprehensive Cancer Center, Georgetown University, Washington, DC 20057, USA. [7]Department of Anatomy and Cell Biology, University of Oviedo, Oviedo, Asturias 33006, Spain. [8]Department of Clinical Neurological Surgery, University of Miami, Miami, FL 33136, USA. [9]Department of Pathology and Laboratory Medicine, Medical University of South Carolina, Charleston, SC 29425, USA. [10]Hollings Cancer Center, Medical University of South Carolina, Charleston, SC 29425, USA.
*Corresponding author. Email: rblanco@musc.edu

with SMO inhibitors (*14*, *16*) might derive from the propagation of a vismodegib-resistant SOX2$^+$ population, which is targetable by inhibiting SHH signaling at the level of GLI. Accordingly, treatment with a clinically relevant GLI inhibitor not only depleted SOX2$^+$ MB cells from tumor tissues but also increased the overall survival of mice harboring MB.

RESULTS

A subset of SOX2$^+$ MB cells express biomarkers indicative of functional SHH signaling

Because of their resistance to SMO inhibition (*19*), we hypothesized that SOX2$^+$ cells display low basal expression of SHH biomarkers, suggesting a nonfunctional pathway. Differential expression analyses for SHH pathway biomarkers using transcriptional data from a *Sox2-eGFP; Ptch1*$^{+/-}$ mouse MB model (*19*) were performed. Although expression of some components of the SHH signaling pathway appears to be down-regulated in SOX2$^+$ sorted cells, statistically significant differences were only found in zinc finger protein of the cerebellum 2 (Zic2), whose expression was lower in SOX2$^+$ cells (Fig. 1A and fig. S1). These data suggest that SOX2$^+$ MB cells might retain some level of SHH signaling activation. Accordingly, 41 and 61% of SOX2$^+$ MB cells found in *Ptch1* and in *Smo* mutant tumors, respectively, were also labeled for a major SHH activator, GLI2 (Fig. 1B and figs. S2, A to D, and S3A). Similar double-labeled cells (19% in RCMB18 and 24% in SJSHHMB-14-7196 (SJSHHMB) were found in two different SHH subgroup patient-derived orthotopic xenografts (PDOXs) and in a human MB tumor microarray (TMA) (Fig. 1B and fig. S3, A and B). In this TMA, 35% of biopsies showed broad nuclear GLI1, which is consistent with the frequency of patients with SHH subgroup MB (*2*). Eighty-five percent of these GLI1$^+$ biopsies were also positive for GLI2, and 66% of these GLI1/2$^+$ tissues harbored SOX2$^+$ cells also expressing GLI2 (21% of the SOX2$^+$ cell count) (fig. S3, B and C). Together, these data indicate that, despite the heterogenicity found in human disease, in more than the half of GLI-expressing MB tumors, a subset of SOX2$^+$ cells express biomarkers suggestive of an active SHH signaling pathway.

To better characterize this SOX2$^+$ cell population expressing biomarkers suggestive of SHH signaling activation, we explored previously generated scRNA-seq data (*20*). Analyses performed in a *Smo*-driven mouse MB model (*SmoM2-eYFP*$^{loxP/loxP}$*; Math1-Cre*) indicated that *Sox2* expression was mainly localized in two independent cell clusters with either an oligodendrocyte- or an astrocyte-like transcriptome (Fig. 1C) (*20*). Although some cells expressing SHH biomarkers might fall under the threshold of detection in scRNA-seq analyses, expression of SHH biomarkers was detected not only in the previously described proliferative nodes A and B (*20*) but also in the *Sox2*-enriched astrocyte compartment (Fig. 1D). Presence of *Sox2*$^+$ astrocytic cells in SHH MB was confirmed upon staining mouse- and human-derived MB tissues for SOX2 and astrocyte markers (Fig. 1E and fig. S4A). Moreover, although, in our TMA, the presence of SOX2$^+$ cells expressing the astrocyte marker glial fibrillary acidic protein (GFAP) was not unique to GLI1/GLI2$^+$ biopsies, in these tissues, ~25% of SOX2$^+$ cells were also expressing GFAP (Fig. 1E and fig. S3, B and C).

Because the expression of SHH biomarkers, astrocytic *Sox2*$^+$ MB cells might be driven by SHH signaling. Analyses of similar publicly available scRNA-seq data obtained from MB harboring *SmoM2* mice treated with either vehicle or vismodegib (*20*) showed a decrease in cells expressing *Sox2* in nodes A and B, as well as in the oligodendrocytic cluster, while an increase was observed in the astrocyte-like one (Fig. 1F), suggesting that these cells are resistant to vismodegib. In these tumor tissues, a reduction in levels (fig. S4B) and percentages (fig. S4, C and D) of either *Gli1*$^+$ or *Gli2*$^+$ cells in nodes A and B, as well as in the *Sox2*-enriched oligodendrocytic cluster was observed. In contrast, examination of the astrocytic compartment revealed an increase of *Gli1/Gli2*-expressing cells (Fig. 1G). Further supporting their resistance to vismodegib, MB tissues exposed to this compound showed an increase in *Sox2/Gli1/Gli2* expression density in the astrocytic cluster (Fig. 1H). These data reveal that vismodegib enriches MB tissues for a population of SMO inhibitor–resistant astrocyte-like *Sox2*$^+$ cells that seems to retain SHH signaling.

GLI signaling drives the growth of SOX2-enriched MB cultures

As activation of SHH signaling downstream of SMO is a common mechanism of resistance to vismodegib in MB and basal cell carcinoma (*16*, *17*), we hypothesized that in SOX2$^+$ MB cells, SHH signaling is activated in a noncanonical manner downstream of SMO. To test this, we used previously described MPC cultures isolated from a *Ptch1-LacZ; Trp53 KO* murine MB model and enriched for SOX2 expression (*22*). Recapitulation of our scRNA-seq analyses showed that a percentage of the SOX2$^+$ cells in culture also exhibited GFAP, GLI1, and GLI2 labeling (Fig. 2A). Despite expressing SHH downstream effectors, concentrations of SMO inhibitors affecting the viability of vismodegib-sensitive SHH MB cells (fig. S5A) (*27*, *28*) had minimal effects on MPC culture proliferation and did not result in increased apoptosis (Fig. 2B and fig. S5B). These results, as well as data from other previously reported research (*18*, *19*, *22*), supported our scRNA-seq analyses, suggesting that SOX2$^+$ MB cells are resistant to SMO inhibition. To determine whether activation of SHH signaling in SOX2$^+$ cells occurs downstream of SMO, we exposed MPC cultures to GLI antagonist-61 (GANT-61), a hexahydropyrimidine derivative, which inhibits GLI1- and GLI2-driven transcription (*26*). GANT-61 attenuated the expression of the SHH target genes (Fig. 2C) and GLI1 and GLI2 levels (fig. S5C), while it reduced the viability of these cultures (Fig. 2D). Moreover, an additional GLI inhibitor, I-BET bromodomain inhibitor 151 (BET151), which blocks SHH signaling by impeding the binding of the bromodomain containing 4 (BRD4) protein to the *Gli1* locus (*23*–*25*), similarly reduced SHH target gene expression (Fig. 2E) and decreased the number of viable MPCs (Fig. 2F); at the same concentrations, it was previously shown to block SHH signaling (*23*, *25*, *29*). Specifically, I-BET151 reduced the ability of these cultures to proliferate and increased apoptosis (Fig. 2G and fig. S5D), which reduced not only the overall numbers of SOX2$^+$ cells in culture but also those coexpressing GLI1, GLI2, and GFAP (Fig. 2H). Consistent with I-BET151 targeting the vismodegib-resistant astrocyte-like *Sox2*$^+$ cells identified in our scRNA-seq analyses, this compound reduced the percentage of MPCs expressing astrocyte and SHH biomarkers (Fig. 2I and fig. S5E).

To validate our GLI inhibitor data, we attenuated the expression of *Smo* and the downstream SHH effectors, *Gli1* and *Gli2*, in MPC cultures using pooled *siRNA* sequences. Silencing *Smo* (fig. S5F) had minimal effects on the expression of SHH target genes (Fig. 2J). However, silencing *Gli2* (fig. S5G) attenuated expression of *Gli1* and *Ptch2* (Fig. 2J), while *Gli1* silencing down-regulated *Ptch2* expression (Fig. 2J) without affecting *Gli2* (fig. S5H). Consistent

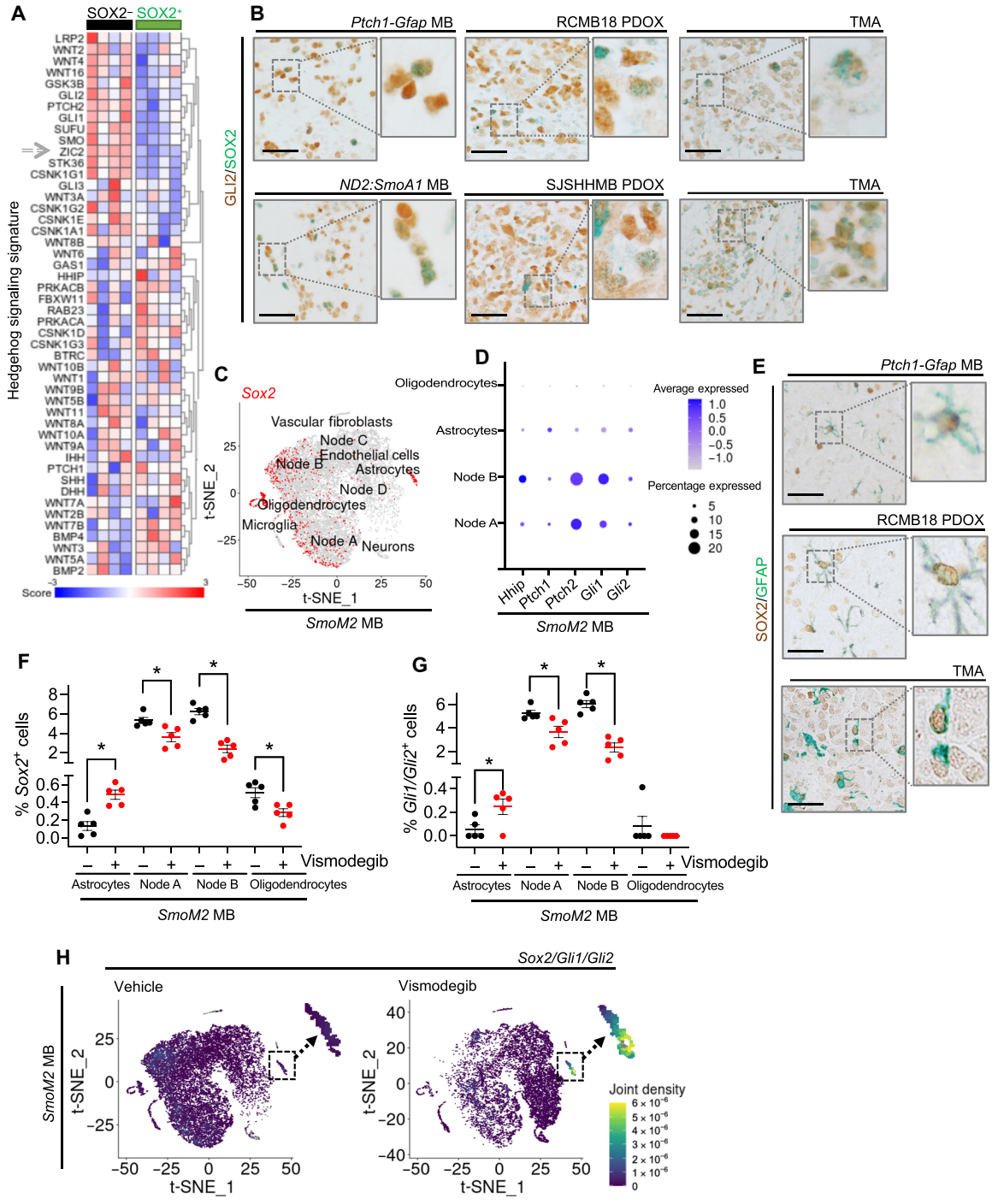

Fig. 1. A subset of SOX2$^+$ MB cells express biomarkers indicative of functional SHH signaling. (**A**) Gene expression profiling from SOX2-eGFP$^+$ and eGFP$^-$ sorted cells isolated from tumors developed in *eGFP-Sox2; Ptch1*$^{+/-}$ mice (RNA-seq data obtained from Dirks, 2014 dataset) was analyzed using a Kyoto Encyclopedia of Genes and Genomes (KEGG) Hedgehog signaling signature. A heatmap comparing gene expression is shown. Arrowhead indicates differentially expressed gene ($P = 0.014$). (**B**) Spontaneous MB tissues developed in *Ptch1-Gfap* or *ND2:SmoA1* mice, two independent PDOX-derived tissues [SJSHHMB-14-7196 (SJSHHMB) and RCMB18], or a human MB TMA were stained for GLI2 and SOX2. (**C**) Expression of *Sox2* in a t-SNE projection of cells was visualized by analyzing previously run scRNA-seq data from spontaneous *SmoM2* MB (sequencing data from Ocasio, 2019 dataset). (**D**) A similar scRNA-seq dataset was used to show expression of SHH biomarkers across indicated nodes. (**E**) Spontaneous MB developed in *Ptch1-Gfap* mice, from mice harboring an SHH subgroup PDOX (RCMB18) or from a TMA were stained for SOX2 and GFAP. (**F**) Percentages of *Sox2*$^+$ cells from *SmoM2* tumors treated with vehicle or vismodegib in the indicated cell clusters were obtained using Ocasio's transcriptomic data. The numbers of *Sox2*$^+$ cells were normalized to total sample cell count. Data shown represent the average percentage for each sequenced tumor. (**G**) Percentages of *Gli1/Gli2*$^+$ cells in vehicle or vismodegib-treated *SmoM2* tumors were similarly calculated. (**H**) A density blot showing *Gli1/Gli2/Sox2* expression in a t-SNE projection of cells from similarly treated tumors. Square details density on astrocytic cluster. Representative IHCs, with highlighted double-labeled cells, are shown. Scale bars, 50 μm. *$P \leq 0.05$.

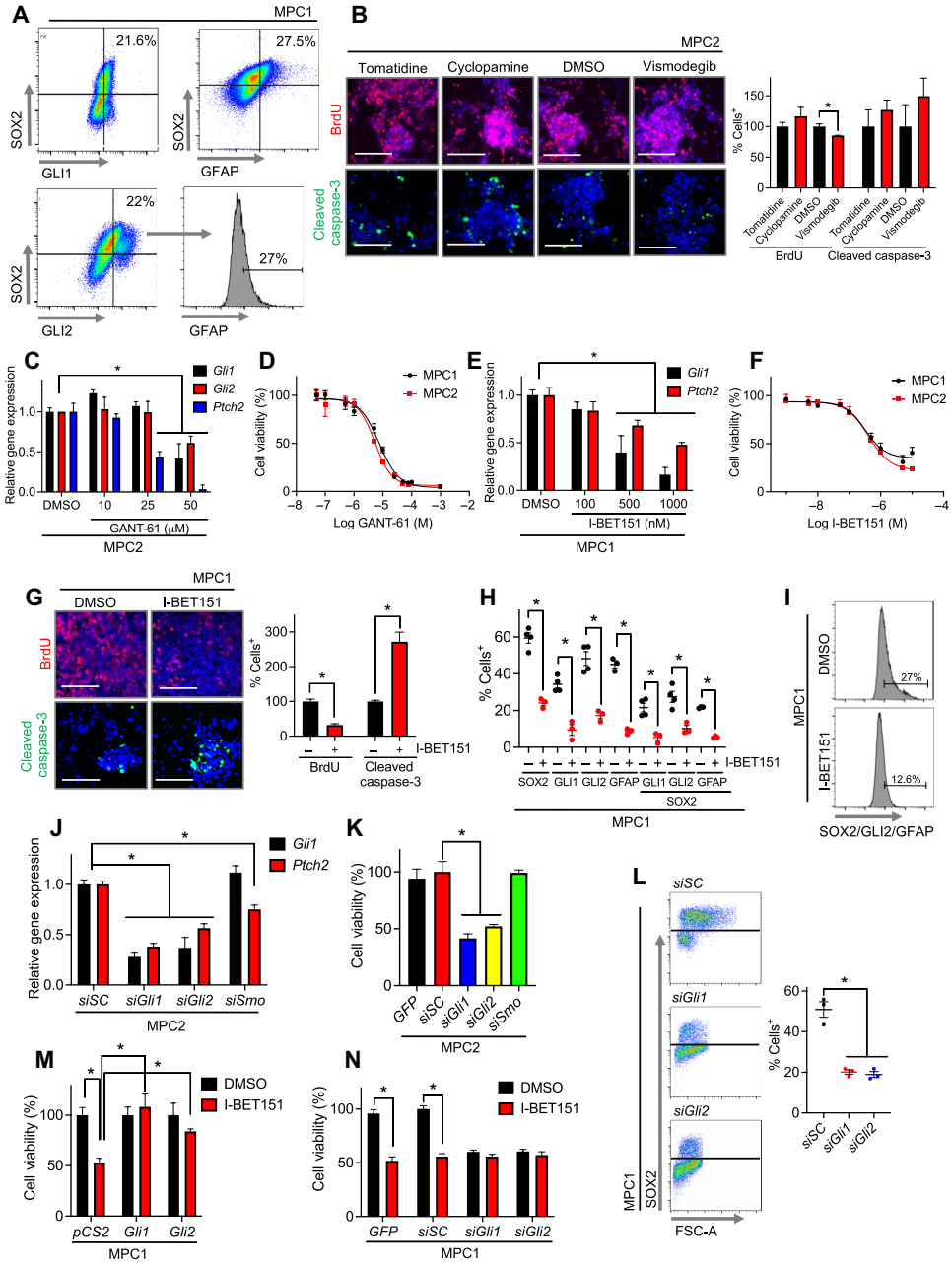

Fig. 2. GLI signaling drives the growth of SOX2-enriched MB cultures. (**A**) Indicated proteins were stained in MPC1 cultures, and percentages of positive cells were determined by flow cytometry analyses. (**B**) MPC2 cultures were exposed to cyclopamine (10 μM) or its inactive analog tomatidine (10 μM), vismodegib (100 nM), or dimethyl sulfoxide (DMSO) for 16 hours before staining for bromodeoxyuridine (BrdU) and cleaved caspase-3. (**C**) MPC2 cultures were exposed to GANT-61 for 16 hours, and expression of indicated genes was determined. (**D**) Indicated cultures were exposed to GANT-61 for 72 hours before determining cell viability by MTT [3-(4,5-dimethyl-2-thiazolyl) 2,5-diphenyl-2*H*-tetrazolium bromide] reduction. (**E**) MPC1 cultures were exposed to I-BET151 for 16 hours before determining the expression of indicated genes. (**F**) MPC cultures were exposed to I-BET151 for 72 hours before determining cell viability by MTT reduction. (**G**) MPC1 cultures were exposed to I-BET151 (500 nM) for 16 hours before assay BrdU incorporation and cleaved caspase-3 expression. (**H**) MPC1 cultures were exposed to I-BET151 (500 nM) for 24 hours, and percentages of positive cells were determined by flow cytometry. (**I**) Percentage of GFAP$^+$ cells in a SOX2/GLI2$^+$ pool was similarly determined. (**J**) MPC2 cultures were transfected with pooled Genome *siRNA* sequences targeting the indicated genes or a scramble siRNA control (*siSC*), and expression of SHH target genes was determined 72 hours later. (**K**) MPC2 cultures were transfected with similar *siRNAs* or a *GFP*-labeled siRNA. Cell viability was determined 5 days later by MTT reduction. (**L**) MPC1 cells were similarly transfected, and numbers of SOX2$^+$ cells were determined by flow cytometry. (**M**) MPC1 cultures were transfected with indicated vectors and, 48 hours later, exposed to I-BET151 (500 nM) for additional 72 hours. Cell viability was determined by MTT reduction. (**N**) MPC1 cultures were transfected with indicated Genome *siRNA* sequences. Forty-eight hours after transfection, cells were exposed to I-BET151 (500 nM) for additional 72 hours, and cell viability was similarly determined. Scale bars, 100 μm. *$P \leq 0.05$.

with the notion that GLI signaling controls the proliferation of SOX2-enriched MPC cultures, attenuation of *Gli1* and *Gli2*, but not *Smo*, partially reduced the number of viable MPC cells (Fig. 2K). Incomplete reduction of numbers of viable cells in these experiments might be due to a partial gene knockdown (Fig. 2J and fig. S5, F to H), likely resulting from a suboptimal transfection rate in sphere cultures or by the presence of a subset of non–GLI-expressing cells in MPC cultures as shown in Fig. 2A. Validating the on-target effect of our small interfering RNA (siRNA) data, an independent set of siRNA pooled sequences targeting *Gli1* and *Gli2* similarly reduced SHH target gene expression (fig. S5, I and J) and the viability of MPC cultures (fig. S5K). Last, flow cytometry analyses showed that, like I-BET151, siRNA targeting either *Gli1* or *Gli2* reduced the numbers of $SOX2^+$ cells in culture (Fig. 2L). Besides *Gli1*, BET inhibition regulates the promoter activity of other well-known oncogenes (*30*–*32*). Thus, to determine whether I-BET151 acts on GLI in our system, we either overexpressed or silenced the positive SHH regulators *Gli1* and *Gli2* in MPC cultures before quantifying the effect of I-BET151 on cell viability. Overexpression of any of these GLI family members rescued the effect of this BET inhibitor in cell viability (Fig. 2M). In contrast, silencing of either *Gli1* or *Gli2* on MPC cultures did not have an additive effect to that of I-BET151, suggesting that this drug is targeting a GLI-dependent cell population (Fig. 2N). Together, these data suggest that the proliferation of SOX2-enriched MB cultures might require noncanonical SHH signaling involving GLI transcription factors.

Activation of GLI signaling in SOX2-enriched MB cultures is dependent on MYC

Previous evidence suggests that an increase in the tumor oncogenic load, elicited by the gain of oncogenes or the loss of a tumor suppressor such as P53, triggers noncanonical GLI signaling (*10*, *12*, *33*–*35*). Our previous data in MPC cultures were performed in cells isolated from *Ptch1-LacZ; Trp53 KO* mice (MPC1 and MPC2). We therefore studied whether activation of SHH signaling downstream of SMO was unique to cultures lacking *Trp53*. GLI inhibition using GANT-61 or I-BET151 reduced the proliferation (Fig. 3A) and SHH target gene expression (Fig. 3, B and C) of MPC cultures isolated from an MB developed in *Ptch1-LacZ* mice that are wild type (WT) for *Trp53* (MPC47). Moreover, *siRNA*-mediated knockdown of *Gli1* or *Gli2*, but not that of *Smo*, also reduced SHH biomarkers (Fig. 3D and fig. S6A) and proliferation (Fig. 3E) on similar WT *Trp53* cultures. Thus, the loss of *Trp53* does not seem to be required to trigger noncanonical GLI signaling in SOX2-enriched MPC cultures.

In addition to loss of P53, noncanonical activation of GLI signaling might be triggered by oncogenes including MYC (*10*, *35*, *36*). Thus, we studied whether MYC could be regulating GLI signaling in SOX2-enriched MB cultures. Inhibition of MYC transcriptional activity using the small-molecule inhibitor 10048-F4, which blocks the binding of MYC to its binding partner MAX (*37*), reduced expression of SHH target genes in our SOX2-enriched MPC cultures (Fig. 3F). This molecule also reduced MPC culture proliferation (Fig. 3G) at concentrations similar to those described before to block MYC signaling (*37*–*39*). Validating 10048-F4 data, attenuation of *Myc* expression using two independent siRNA smart pools (Fig. 3H and fig. S6B) reduced the expression of SHH target genes in these cells (Fig. 3I and fig. S6B), as well as their overall viability (Fig. 3J and fig. S6C) and specific numbers of SOX2 expressing cells (Fig. 3K). Similar reduction in SHH target genes (fig. S6D) was observed by using a CRISPR-Cas9–mediated approach to silence *Myc* (fig. S6E). In line with a vismodegib-resistant astrocyte-like $SOX2^+$ population in which noncanonical SHH signaling is activated by MYC, in spontaneous *SmoA1* mutant MB tissues, expression of MYC was found in a small number of cells labeled for the astrocyte biomarker GFAP and in $SOX2^+$ cells (Fig. 3L). Moreover, while our analyses of scRNA-seq data performed in *SmoM2* mice showed a reduction in *Myc* expression on proliferative nodes A and B in tumors exposed to vismodegib (fig. S6F), a specific enrichment in *Sox2/Gli1/Gli2/Myc* density in the astrocytic cluster was observed (Fig. 3M). As illustrated in Fig. 3N, these results show that, although additional signaling mechanisms might be involved, MYC seems to activate SHH signaling downstream of SMO in SOX2-enriched MPC cultures.

In vivo inhibition of SHH signaling downstream of SMO depletes $SOX2^+$ MB cells

We have shown that SHH MB harbors a $SOX2^+$ subpopulation that is resistant to SMO inhibitors but relies on GLI signaling for ex vivo growth. We therefore studied whether attenuation of SHH signaling downstream of SMO would similarly target this $SOX2^+$ cell population in vivo. Freshly isolated MB cells from *Ptch1-LacZ* and *Ptch1-LacZ; Trp53 KO* mice devoid of any expansion in culture were subcutaneously implanted in mice. Because of the mixed genetic background of these cells, immunocompromised mice were used. SHH signaling was inhibited at the level of GLI in these mice by administrating I-BET151 (Fig. 4A). As proliferation of these tumors is driven by lack of PTCH1 activity (*9*), MB growth was significantly reduced by this drug (Fig. 4B). In I-BET151–treated mice, the overall SOX2 levels (Fig. 4A) and the number of $SOX2^+$ cells (Fig. 4C) were reduced in residual tumors. These data suggest that inhibition of SHH signaling downstream of SMO depletes a $SOX2^+$ population in vivo. Because I-BET151 can regulate the activity of several promoters (*30*–*32*) and therefore might be acting independently of GLI in vivo, we treated similar *Ptch1-LacZ* mutant tumors with the functionally different GLI inhibitor Gant-61 (*26*). Similar to I-BET151, Gant-61 attenuated tumor growth (Fig. 4D) and reduced the levels of the final SHH effectors GLI1 and GLI2, as well as overall SOX2 levels (Fig. 4E) and cell numbers (Fig. 4F).

GLI inhibition attenuates SHH MB progression

Given that neither I-BET151 (*40*) nor Gant-61 (*41*) are likely to cross the blood-brain barrier, limiting their efficacy to subcutaneous MB models, we turned to the drug JQ-1 as an alternative BET inhibitor, which could demonstrate efficacy in the brain (*42*). Similar to I-BET151 or Gant-61, JQ-1 attenuated the proliferation (Fig. 5A) and inhibited SHH signaling (Fig. 5B) of $SOX2^+$ cell–enriched MPC cultures and did this, at least in part, via a GLI-dependent manner (fig. S7A). Consistent with an SHH inhibitor, in a *Ptch1-LacZ* in vivo MB model, JQ-1 reduced the expression of SHH biomarkers (Fig. 5C) and target genes (Fig. 5D). When comparing the activity of JQ-1 to that of vismodegib, both decreased the size of similar SHH-driven tumors, either when implanted subcutaneously (Fig. 5E) or orthotopically in the brain (Fig. 5F). Consistent with our scRNA-seq analyses, a significant enrichment in cells expressing SOX2 was observed in vismodegib treated tumors (Fig. 5G). On the contrary, tumor tissues exposed to JQ-1 showed a reduction in number (Fig. 5G) and overall protein levels (Fig. 5C) of SOX2. Flow cytometry analyses performed in mice exposed to either vehicle or JQ-1

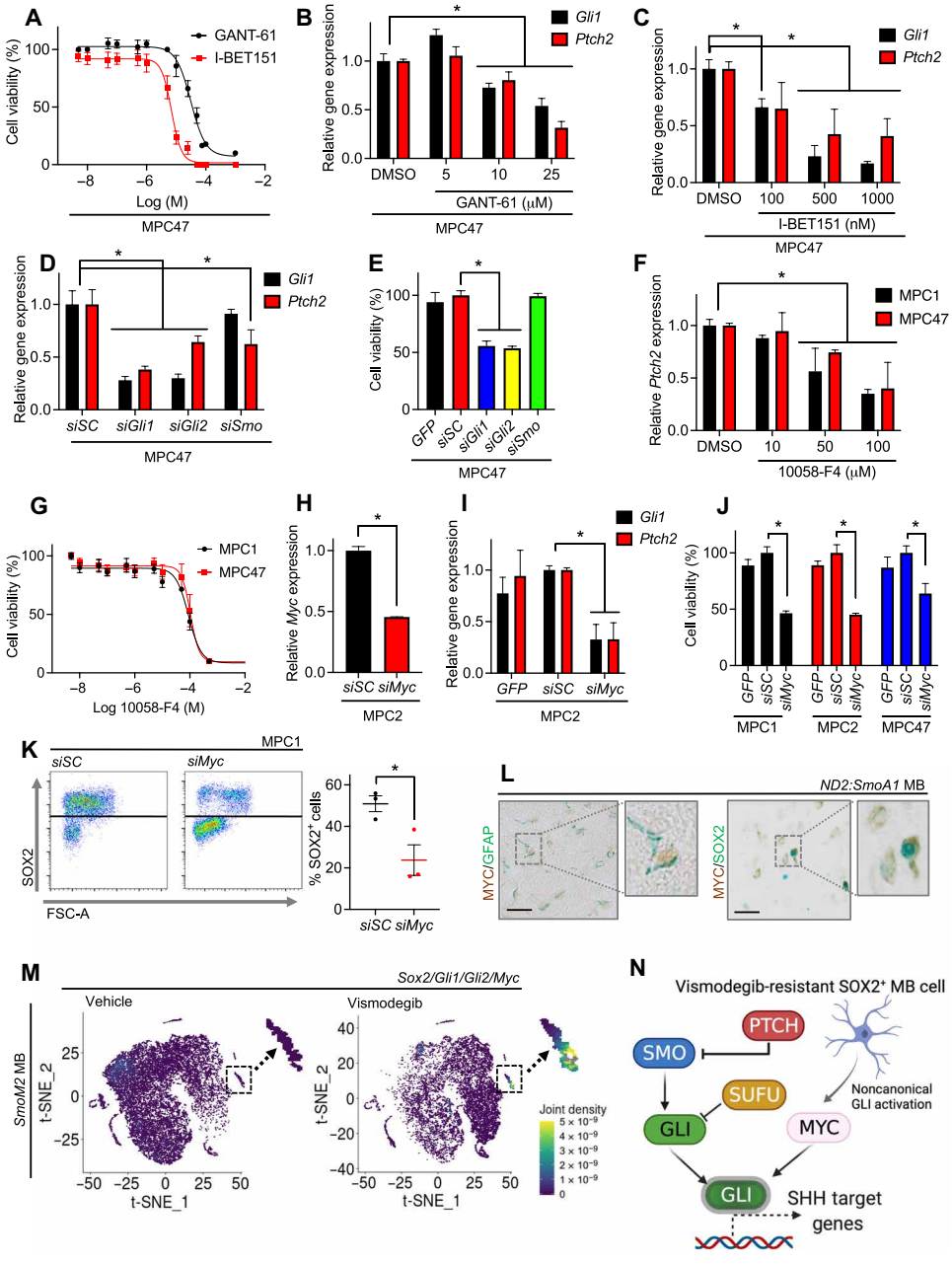

Fig. 3. Activation of GLI signaling in SOX2-enriched MB cultures is dependent on MYC. (**A**) MPC47 cultures were exposed to GANT-61 or I-BET151 for 72 hours, and cell viability was determined by MTT reduction. (**B**) MPC47 cultures were exposed to GANT-61 for 16 hours, and expression of indicated genes was determined. (**C**) MPC47 cultures were exposed to I-BET151 for 16 hours, and SHH target gene expression was determined by RT-qPCR. (**D**) MPC47 cultures were transfected with indicated pooled Genome *siRNA* sequences, and expression of indicated genes was similarly determined 72 hours later. (**E**) MPC47 cultures were transfected with similar *siRNA* sequences or a *GFP-siRNA*. Cell viability was determined 5 days later by MTT reduction. (**F**) MPC cultures were exposed to 10058-F4 for 16 hours, and SHH target gene expression was determined. (**G**) Indicated cultures were exposed to 10058-F4 for 48 hours before determining cell viability by MTT reduction. (**H**) MPC2 cultures were transfected with pooled Genome *siRNA* sequences, and expression of *Myc* was determined 72 hours later. (**I**) MPC2 cultures were transfected with similar *siRNA* sequences, and expression of indicated genes was determined 72 hours later. (**J**) MPC cultures were similarly transfected, and cell viability was determined 5 days later by MTT reduction. (**K**) MPC1 cultures were transfected with pooled Genome *siRNA* sequences for 5 days before quantify percentages of $SOX2^+$ cells by flow cytometry. (**L**) Indicated proteins were stained in *ND2:SmoA1* brains. Square details double-positive cell in a representative image. Scale bars, 50 μm. (**M**) scRNA-seq data from *SmoM2* mice exposed to vehicle or vismodegib (Ocasio's dataset) were used to study the density of *Sox2/Gli1/Gli2/Myc* expression in a t-SNE plot. (**N**) Schematic of canonical and MYC-driven noncanonical SHH signaling in $SOX2^+$ MB cells. $^*P \leq 0.05$.

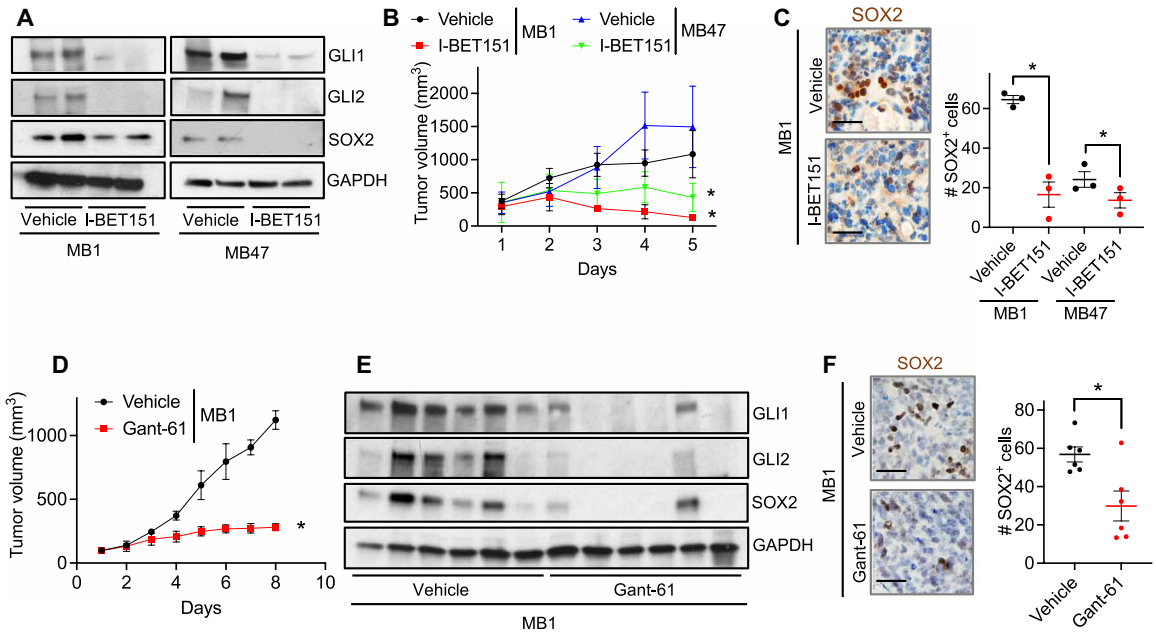

Fig. 4. In vivo inhibition of SHH signaling downstream of SMO depletes SOX2$^+$ MB cells. (**A**) Spontaneous tumors developed in *Ptch1-LacZ;Trp53-KO* (MB1) or *Ptch1-LacZ* (MB47) mice were subcutaneously implanted into mice. Once the tumor size reached approximately 100 mm^3, mice were treated with I-BET151 [30 mg/kg, intraperitoneally (i.p.), daily (q.d.)] or vehicle for 5 days, and levels of indicated proteins were determined by immunoblotting. (**B**) Tumor volume was measured in similarly treated mice. (**C**) MB1 and MB47 tumor tissues were similarly exposed to I-BET151, and residual tumors were stained for SOX2 and number of positive cells per field quantified. (**D**) Mice harboring MB1 subcutaneous tumors were treated with Gant-61 (40 mg/kg, subcutaneously, every other day) or vehicle for 8 days. Tumor volume was measured every other day. (**E**) Mice harboring MB1 tumors were similarly exposed to Gant-61, and levels of indicated proteins were determined by immunoblotting. (**F**) MB1 tumor tissues were similarly exposed to Gant-61; residual tumors were stained for SOX2, and the number of positive cells per field was quantified. Representative images are shown. Scale bars, 50 μm. *$P \leq 0.05$.

showed similar decrease in numbers of SOX2$^+$ cells, including those expressing either GLI1 or GLI2 (Fig. 5H). Last, consistent with JQ-1 targeting the previously described pool of astrocyte-like SOX2$^+$ cells, this BET inhibitor also depleted from tumors those SOX2$^+$ cells labeled with astrocyte and SHH biomarkers (Fig. 5I). These results further suggest that SHH MB harbors a pool of vismodegib-resistant SOX2$^+$ MB cells that can be targeted by inhibiting SHH signaling downstream of SMO.

Given that vismodegib-treated patients tend to relapse (*14*–*17*), we questioned whether the vismodegib-resistant SOX2/GLI$^+$ cell population was the underlying reason for tumor regrowth and whether attenuation of SHH signaling downstream of SMO would impede it. To test this, mice harboring subcutaneous *Ptch1-LacZ* MB were dosed with vismodegib, JQ-1, or vehicle control for 8 days before the harvest of residual tumor tissues. An equal number of viable cells from these tumors were subsequently either plated or orthotopically implanted (Fig. 5J). Treatment with JQ-1 reduced primary sphere formation, while vismodegib-treated residual tumors promoted a greater number of spheres compared to vehicle-treated tissues (Fig. 5K). Similar to this ex vivo observation, JQ-1 treatment partly prevented secondary tumor engraftment, while mice implanted with residual vismodegib-treated tumors had a worse outcome compared to their vehicle-treated counterparts (Fig. 5L). As high expression of *SOX2* correlates with poor outcomes in patients with MB (*19*), we studied whether tumors grown from vismodegib preexposed tissues in Fig. 5L overexpressed SOX2. Such reengrafted tumors were indeed enriched in cells expressing SOX2 compared to those treated with JQ-1 or vehicle (fig. S7B). Collectively, our data show that vismodegib-exposed residual MB gives rise to aggressive SOX2$^+$ cell–enriched tumors, whose propagation could be prevented by inhibiting SHH signaling downstream of SMO. Moreover, according to our observations in mouse MB tissues, treatment of mice harboring an SHH subgroup PDOX with JQ-1 similarly reduced the number of SOX2$^+$ cells while vismodegib failed to do so (Fig. 5M).

The BET inhibitor BMS-986158 attenuates SHH signaling and *Ptch1* driven MB growth

Our data suggest that, because of the depletion of the SOX2 cell population from tumors, inhibition of SHH signaling at the level of GLI would provide a more stable disease remission than targeting SMO. Limiting the translational relevance of our data, none of the GLI inhibitors used thus far have a pharmacokinetic profile suitable for brain tumor patients, as neither I-BET151 (*40*) nor Gant-61 (*41*) are brain penetrant and JQ-1 has a short half-life (*43*). Therefore, we studied whether the BET inhibitor, BMS-986158, currently undergoing clinical evaluation on pediatric and adult malignancies (NCT02419417, NCT03936465, and NCT04817007) could similarly block SHH signaling at the level of GLI and therefore provide long-lasting MB remission. Low nanomolar concentrations of this compound attenuated *Gli1* promoter activity in an SHH reporter cell line (Fig. 6A), as well as the expression of the SHH biomarker GLI1 (Fig. 6B) and SHH target genes (Fig. 6C) in immortalized mouse embryonic fibroblasts (MEFs) (*44*) in which SHH signaling was induced by using an SMO agonist (SAG). Consistent with its predicted mechanism of action on GLI, BMS-986158 also attenuated SHH signaling in immortalized MEFs lacking *Sufu* expression

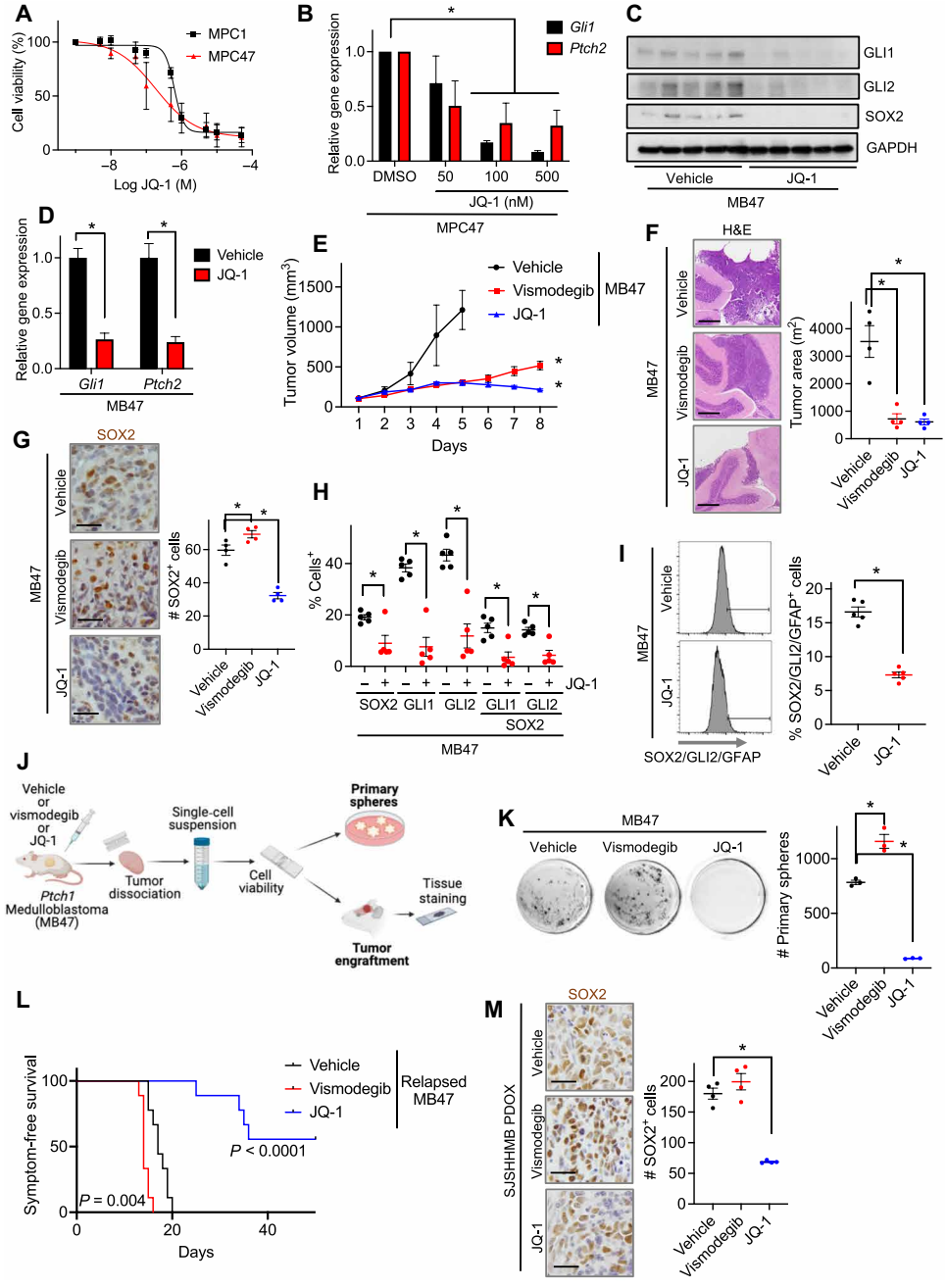

Fig. 5. GLI inhibition attenuates SHH MB progression. (**A**) MPC cultures were exposed to JQ-1 for 72 hours before determining cell viability by MTT reduction. (**B**) MPC47 cells were exposed to JQ-1, and expression of indicated genes was determined 16 hours later. (**C**) Mice harboring *Ptch1-LacZ* (MB47) subcutaneous tumors were treated with JQ-1 (30 mg/kg, i.p., q.d.) or vehicle for 8 days, before determining levels of the indicated proteins. (**D**) Expression of indicated genes was determined in similarly dosed mice. (**E**) Mice harboring similar tumors were treated with JQ-1 (30 mg/kg, i.p., q.d.), vismodegib (25 mg/kg, i.p., q.d.), or vehicle for 8 days, and the tumor volume was measured. (**F**) Mice harboring orthotopic MB47 tumors were similarly dosed, and tumor area was quantified. Scale bars, 200 μm. (**G**) Number of SOX2$^+$ cells in brain tumors from similarly treated mice were quantified. (**H**) Mice harboring subcutaneous MB47 tumors were treated with vehicle or JQ-1 (30 mg/kg, i.p., q.d.) for 8 days, before determining percentage of positive cells by flow cytometry. (**I**) Percentages of GFAP$^+$ in SOX2/GLI2$^+$ cells were similarly determined. (**J**) Mice harboring subcutaneous MB47 were treated with JQ-1 (30 mg/kg, i.p., q.d.), vismodegib (25 mg/kg, i.p., q.d.), or vehicle for 8 days. Equal numbers of viable cells from residual tumors were then allowed to form spheres ex vivo or to orthotopically engraft in vivo. A schematic of the procedure is shown. (**K**) Numbers of spheres grown from treated tumors described in (J) were quantified. (**L**) Tumor engraftment capability from similar residual tumors was determined. (**M**) PDOX harboring mice were dosed with vehicle, vismodegib (25 mg/kg, i.p., q.d.), or JQ-1 (30 mg/kg, i.p., q.d.) for 8 days, before staining brains for SOX2. Unless otherwise indicated, scale bars, 50 μm. *$P \leq 0.05$.

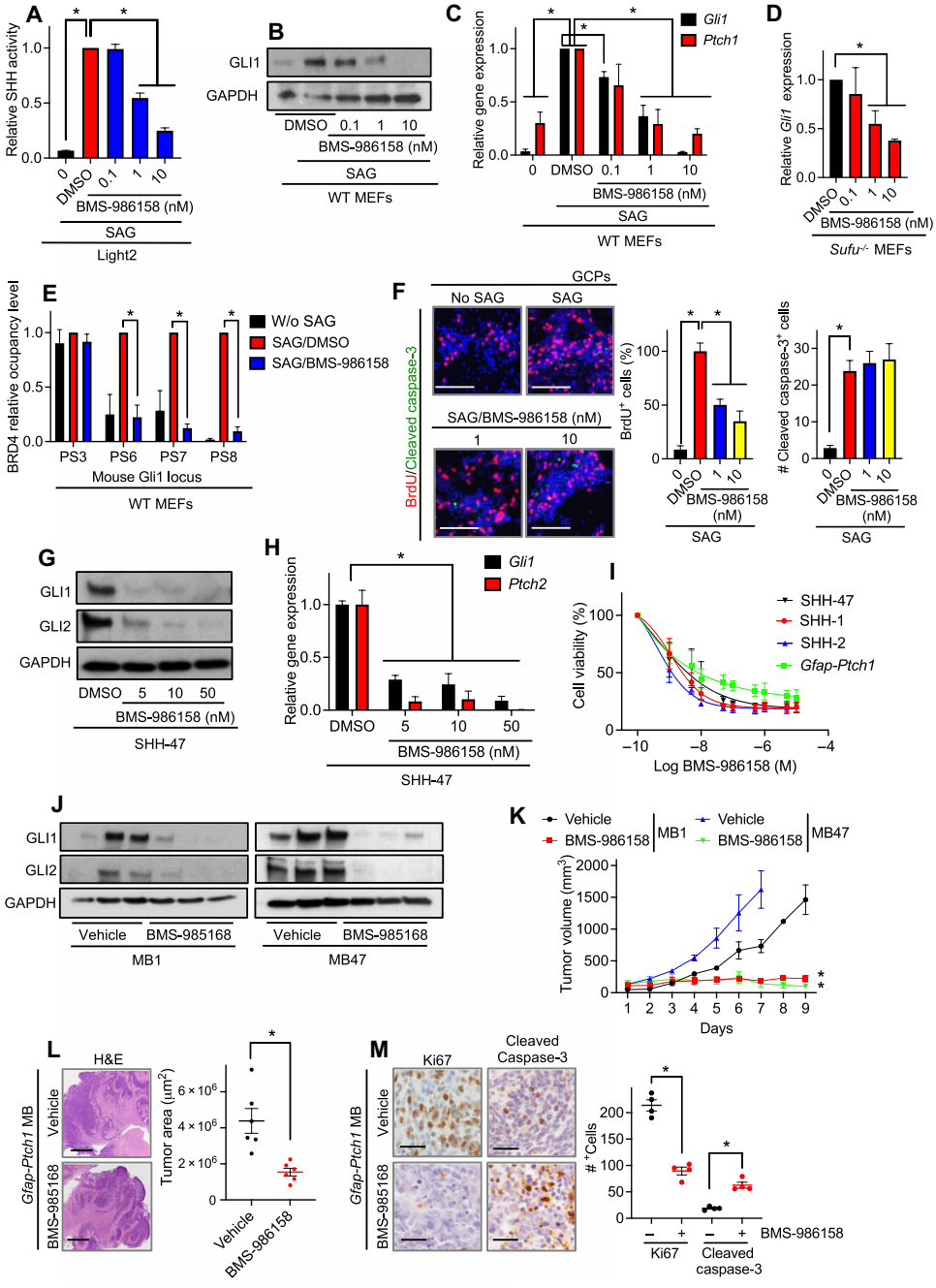

Fig. 6. The BET inhibitor BMS-986158 attenuates SHH signaling and *Ptch1* driven MB growth. (**A**) Light2 cells were exposed to 100 nM SAG for 24 h, before exposing them to BMS-986158. GLI- driven luciferase activity was determined 16 hours later. (**B**) WT MEFs were similarly treated, before immunoblot protein lysates for indicated proteins. (**C**) Expression of the indicated genes in similarly treated MEFs was determined. (**D**) *Sufu*$^{-/-}$ MEFs were treated with BMS-986158 for 16 hours, and *Gli1* expression was determined. (**E**) WT MEFs were treated with SAG (100 nM) for 24 hours before their exposure to BMS-986158 for additional 16 hours. BRD4 occupancy in *Gli1* locus was analyzed by ChIP-PCR and normalized to a ChIP performed using rabbit IgG. Primer set 3 (PS3) was used as a negative control, while PS6 to PS8 aligned with *Gli1* promoter. (**F**) GCPs were induced with 100 nM SAG for 24 hours and exposed to BMS-986158 for additional 16 hours, before assay BrdU incorporation and stain-cleaved caspase-3. Scale bar, 100 μm. (**G**) Vismodegib-sensitive SHH-47 cells were exposed to BMS-986158 for 16 hours, and expression of indicated proteins was determined. (**H**) Expression of indicated genes was assayed in similarly treated cells. (**I**) Indicated cells were exposed to BMS-986158 for 72 hours, and cell viability was determined by MTT reduction. (**J**) Mice harboring subcutaneous MB47 (*Ptch1-LacZ*) and MB1 (*Ptch1-LacZ*, *Trp53-KO*) tumors were dosed with BMS-986158 (3 mg/kg, i.p., q.d.) or vehicle for 8 days, before determining levels of indicated proteins. (**K**) Tumor size in similarly treated mice was determined. (**L**) Ten-day-old *Ptch1-Gfap* mice were dosed for 8 days with vehicle or BMS-986158 (3 mg/kg, i.p., q.d.), and the size of tumors was quantified. Scale bar, 200 μm. (**M**) Brains from similarly treated *Ptch1-Gfap* mice were stained for the indicated proteins. Scale bars, 50 μm. *$P \leq 0.05$.

(*Sufu*$^{-/-}$ MEFs), which therefore harbor SHH signaling constitutively active downstream of SMO (Fig. 6D) (*45*), and reduced the enrichment of BRD4 in the *Gli1* locus (Fig. 6E). This BMS compound also attenuated the proliferation of cerebellar GCPs, which multiply in response to SHH signaling activation without inducing cell death in either induced (Fig. 6F) or uninduced (fig. S7C) GCPs.

In tumor cells, BMS-986158 attenuated SHH signaling (Fig. 6, G and H) and the ex vivo growth (Fig. 6I) of previously described vismodegib-sensitive MB cultures (*27*, *28*). In vivo, this BMS compound similarly reduced levels of SHH signaling biomarkers (Fig. 6J) and abrogated subcutaneous tumor growth (Fig. 6K). In a spontaneous *Ptch1*-driven mouse MB model (*Ptch1-Gfap*), BMS-986158 treatment similarly reduced the size of residual tumors (Fig. 6L), cutting off tumor proliferation, and increased the expression of apoptotic biomarkers (Fig. 6M). Together, these data show that use of a clinically relevant BET inhibitor leads to SHH signaling inhibition at the level of GLI, which, in turn, attenuates in vivo MB growth.

BMS-986158 exhausts a SOX2$^+$ cell population and prevents MB relapse

Because BMS-986158 inhibits SHH signaling at the level of GLI, we speculated that this novel BET inhibitor would prevent SOX2$^+$-driven MB relapse. Similar to the other GLI inhibitors tested, BMS-986158 attenuated SHH signaling (Fig. 7, A and B) and the proliferation (Fig. 7C) of vismodegib-resistant SOX2$^+$ cell–enriched MB cultures, at least in part, via a GLI-dependent manner (fig. S7A). Consistent with our previous in vivo observations, GLI inhibition by BMS-986158 reduced the levels (Fig. 7D) and the number of SOX2 expressing cells (Fig. 7E). Similar to JQ-1, and as illustrated in Fig. 5J, residual tumors isolated from BMS-986158–treated mice made fewer primary spheres compared to those derived from vehicle-treated mice (Fig. 7F) and mostly failed to engraft in vivo (Fig. 7G).

Our scRNA-seq analyses suggested that SHH MB harbors a population of vismodegib-resistant SOX2$^+$ cells with an astrocytic transcriptome. Thus, we wanted to know whether BMS-986158 efficacy correlated with a reduction of the astrocytic SOX2$^+$ cell pool. As we described before, mass cytometry imaging of spontaneous *Ptch1*-driven tumors exposed to BMS-986158 showed a reduction in the expression of GLI2, the proliferation biomarker Ki67, and SOX2 labeling (Fig. 7H). Similar to our previous results in JQ-1–exposed tumors, a reduction of GFAP$^+$ cells that also expressed SOX2 was observed in tissues treated with BMS-986158 (Fig. 7I). Thus, BMS-986158 drains the overall SOX2$^+$ cell population, including astrocytic SOX2$^+$ cells that were previously resistant to vismodegib treatment.

GLI inhibition provides stable tumor remission in SMO inhibitor resistant MB

Because of the mechanism of inhibition of SHH signaling by BMS-986158, we wondered whether it would show efficacy not only in vismodegib-sensitive *Ptch1*-driven MB but also in those that are vismodegib resistant in the clinic (*46*). In a spontaneous *Smo* mutant MB model, BMS-986158 reduced tumor size (Fig. 8A) and proliferation index, while it increased the number of apoptotic cells (Fig. 8B). In these tumors, we observed a reduction in the number of cells expressing the SHH effector GLI2 (Fig. 8B), which is consistent with an attenuation of SHH signaling. Moreover, residual *SmoA1* MB tissues exposed to BMS-986158 had fewer SOX2$^+$ cells than those exposed to vehicle control (Fig. 8B) and showed significantly longer symptom-free survival (Fig. 8C).

Last, we studied the efficacy of BMS-986158 in treatment-resistant *TP53* mutant and *MYCN*-amplified MB tissues, which is considered a very high-risk disease and has the worst outcome within the SHH subgroup of patients with MB (*47*). In these tumors, BMS-986158 reduced tumor size (Fig. 8D) and proliferation index while slightly increasing caspase-3 cleavage (Fig. 8E). Consistent with an SHH inhibitor, this BMS compound also reduced the numbers of cells expressing the SHH biomarkers GLI1 and GLI2 in residual tumor tissues (Fig. 8F). Similar to JQ-1, BMS-986158 reduced the number of SOX2$^+$ MB cells in two independent PDOX models (Fig. 8G). Ultimately, BMS-986158 increased the life span of mice harboring these high-risk PDOX tumors (Fig. 8H), which further emphasized the clinical advantage and translational promise of using compounds that target GLI for the treatment of patients with MB.

DISCUSSION

Here, we show that SHH MB harbors a pool of SOX2-labeled MB cells in which expression of the final SHH signaling effectors *Gli1* and *Gli2* is increased by vismodegib. Consistent with SMO-independent activation of SHH signaling, the proliferation of SOX2-enriched MB cultures is not affected by SMO inhibition but rather by those compounds acting on GLI. According to this observation, in vivo inhibition of SHH signaling downstream of SMO reduces the number of SOX2$^+$ cells, while SMO inhibitors exhibit an opposite effect. In accordance with the key role of SOX2$^+$ cells in propagating MB (*18*, *19*), GLI inhibition reduces the chances of tumor reengraftment, while vismodegib-exposed residual tumors become even more aggressive than their vehicle-treated counterparts. Combined, our results uncover a key driver of the SOX2$^+$ cancer–propagating cell characterized by a noncanonical activation of GLI signaling, which might facilitate tumor propagation and likely underlies treatment resistance and subsequent cancer relapse seen in patients with SHH subgroup MB (*14*, *16*).

Clinical observation of frequent tumor recurrence upon administration of SMO inhibitors (*14*–*17*) suggests that compensatory signaling pathways drive relapse mechanisms. Such relapses could be driven by treatment-resistant tumor-propagating cells labeled by stemness biomarkers. Similar to previous reports (*19*, *20*), we observed that treatment with vismodegib increases the numbers of cells expressing SOX2 in residual tumor tissues. These data suggest that SOX2$^+$ cells are resistant to SMO inhibition. In contrast, our current findings suggest that attenuation of GLI signaling using a clinically relevant BET inhibitor (BMS-986158) not only attenuates vismodegib-sensitive and vismodegib-resistant primary tumor growth but also partially reduces the chances of tumor recurrence. The fact that some tumors preexposed to BET inhibitors did engraft suggests either a partial depletion of the SOX2$^+$ MB pool or additional signaling mechanisms allowing cancer relapse.

Our results in mouse- and human-derived MB models reveal that only a select number of SOX2$^+$ MB cells express biomarkers indicative of SHH signaling activation. Similar GLI expressing SOX2$^+$ cells were found in more than the half of GLI1/GLI2-labeled biopsies in an MB TMA. The partial presence of these cells in GLI$^+$ biopsies might indicate their link to one or more of the four SHH MB subtypes (*47*) or could be used to predict sensitivities to BET inhibitors. Therefore, future analyses should be performed to address whether relapses of GLI$^+$ tissues lacking SOX2/GLI$^+$ cells could be prevented by BET inhibition. According to our scRNA-seq

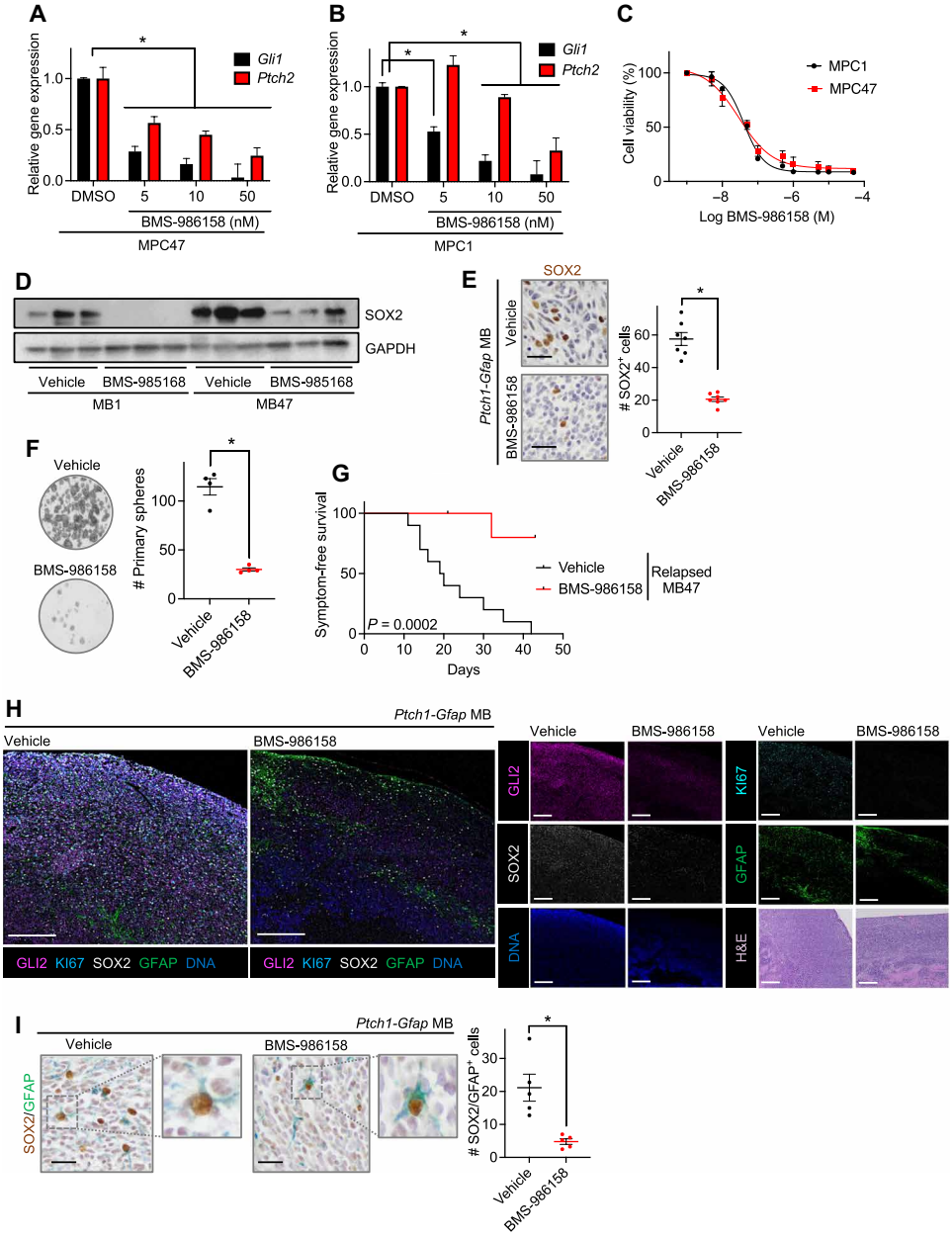

Fig. 7. BMS-986158 exhausts a SOX2$^+$ cell pool and prevents MB relapse. (**A**) MPC47 cultures were exposed to BMS-986158 for 16 hours before determining expression of SHH target genes. (**B**) MPC1 cultures were similarly exposed to BMS-986158, and expression of indicated genes was determined. (**C**) MPC cultures were exposed to BMS-986158 for 72 hours before determining cell viability by MTT reduction. (**D**) Mice harboring subcutaneous MB47 (*Ptch1-LacZ*) and MB1 (*Ptch1-LacZ*, *Trp53-KO*) tumors were exposed to BMS-986158 (3 mg/kg, i.p., q.d.) or vehicle for 8 days, and levels of indicated proteins were determined. (**E**) Ten-day-old *Ptch1-Gfap* mice were treated with vehicle or BMS-986158 (3 mg/kg, i.p., q.d.) for 8 days, and SOX2 was detected by IHC staining. (**F**) Mice harboring subcutaneous MB47 were treated with BMS-986158 (3 mg/kg, i.p., q.d.) or vehicle for 8 days. As shown in Fig. 5J, equal number of viable cells from residual tumors were then allowed to form spheres ex vivo. (**G**) As represented in Fig. 5J tumor engraftment capability from similarly treated tumors was determined. (**H**) Ten-day-old *Ptch1-Gfap* mice were treated with BMS-986158 (3 mg/kg, i.p., q.d.) or vehicle for 8 days before labeling brain tissues with indicated metal conjugated antibodies. Representative multiplexing mass cytometry images and corresponding H&E staining are shown. Scale bars, 200 μm. (**I**) *Ptch1-Gfap* mice were similarly treated before staining brains for SOX2 and GFAP. Unless otherwise indicated, scale bars, 50 μm. *$P \leq 0.05$.

analyses, this subset of SOX2/GLI$^+$ cells harbors an astrocytic signature. Although additional studies are required to better characterize these astrocyte-like SOX2$^+$ MB cells, a similar population of SOX2$^+$ astrocyte progenitors has been shown to promote malignancy in glioblastoma models (*48*) or can be transformed to trigger group 3 MB development (*49*). Further suggesting the key role of astrocyte-like cells in brain neoplasia, in SHH MB, GCPs transdifferentiate into tumor-associated astrocytes, which have been shown to then go on to coordinate with microglia to promote tumor growth (*50*).

The drivers of proliferation of SOX2$^+$ cell–enriched MB cultures may be altered by the presence of trophic factors in growth media. Accordingly, fibroblast growth factor (FGF) blocks SHH signaling

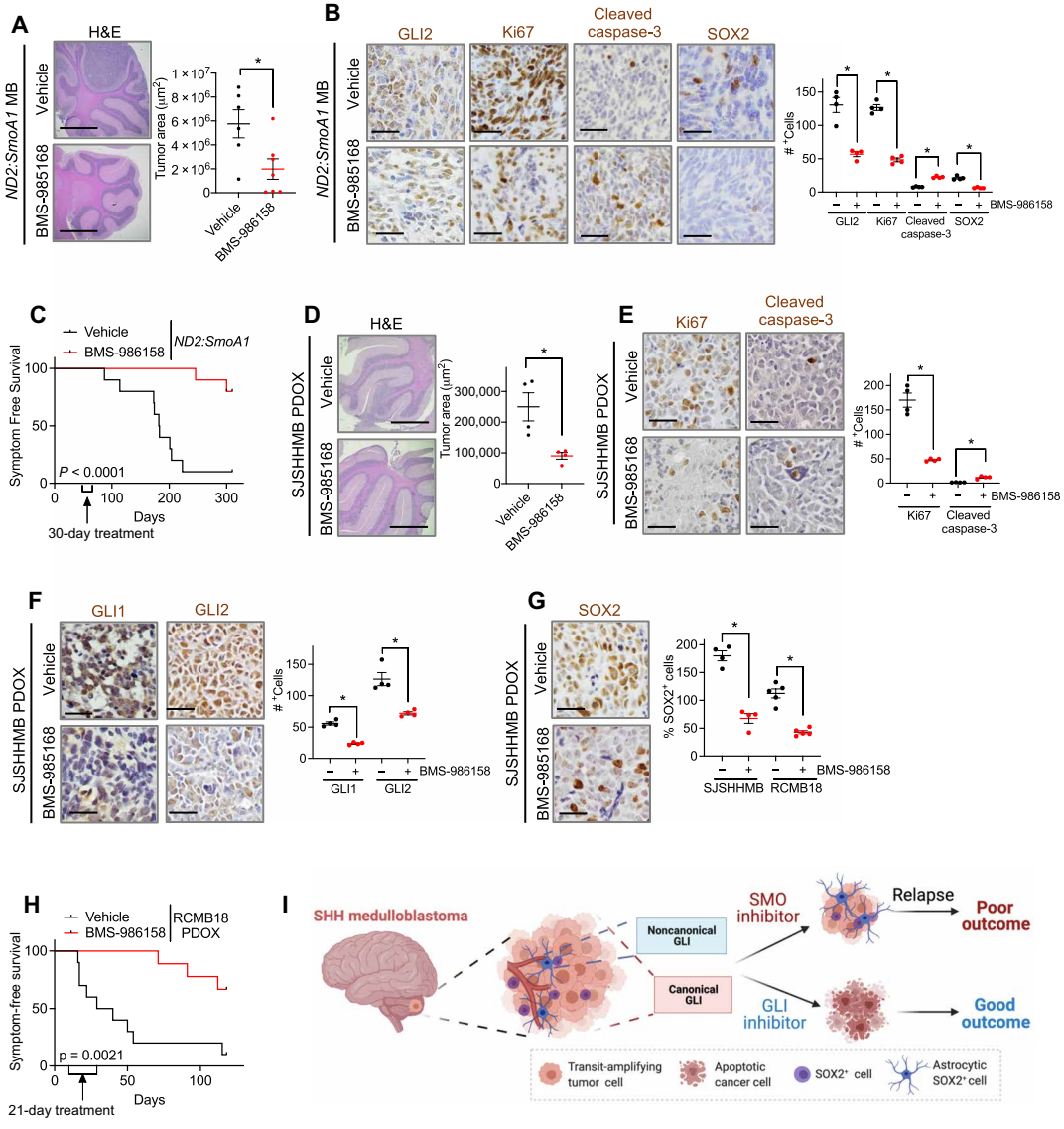

Fig. 8. GLI inhibition provides stable tumor remission in SMO inhibitor-resistant MB. (**A**) Six-month-old *ND2:SmoA1* mice were exposed to BMS-986158 (3 mg/kg, i.p., q.d.) for 8 days. The size of residual tumors was quantified. Scale bars, 200 μm. (**B**) Brains from similarly treated *ND2:SmoA1* mice were stained for indicated proteins, and numbers of positive cells were quantified. (**C**) Two-month-old *ND2:SmoA1* mice were exposed to BMS-986158 (3 mg/kg, i.p., q.d.) or vehicle, and symptom-free survival was determined. (**D**) Three weeks after orthotopically implanting SJSHHMB PDOX cells, mice were exposed to BMS-986158 (3 mg/kg, i.p., q.d.) or vehicle for 8 days before harvesting their brains, and the size residual tumors was measured. Scale bars, 200 μm. (**E**) Mice harboring SJSHHMB PDOX tissues were similarly treated, and brains were stained for indicated proteins. (**F**) Similarly implanted mice were treated with BMS-986158 (3 mg/kg, i.p., q.d.) or vehicle for 8 days before staining tissues for GLI1 and GLI2. (**G**) Mice implanted with either SJSHHMB or RCMB18 PDOX cells were similarly dosed before staining brain tissues for SOX2. (**H**) Mice orthotopically harboring a RCMB18 PDOX were dosed with BMS-986158 (3 mg/kg, i.p., q.d.) or vehicle, and symptom-free survival was determined. (**I**) Model illustrating cell diversity in SHH MB. Unless otherwise indicated, scale bars, 50 μm. *$P \leq 0.05$.

in MB cells (*51*), which may explain why SOX2$^+$ cell–enriched MB cultures grown in FGF-containing media are resistant to SMO inhibitors. Nevertheless, this observation does not explain why in vivo exposure to vismodegib enriches tumor tissues that were never expanded ex vivo for SOX2-expressing cells or why these cells rely on GLI signaling to proliferate. An increase in the tumor oncogenic load might activate GLI signaling in an FGF-independent manner through the activity of oncogenic proteins (*10*). Fittingly, our data suggest, that in SOX2$^+$ MB cells GLI signaling is activated in an MYC-dependent manner. It was previously shown that MYC interacts with the 5′-regulatory region of *GLI1* to control GLI-driven transcription (*35*, *36*) and that this regulation occurs through the interaction of the MYC-interacting zinc finger protein 1 with GLI2 (*52*). Our data reveal that, similar to GLI, attenuation of MYC signaling using an MYC inhibitor blocks the proliferation of SOX2$^+$ cell–enriched MB cultures, signifying that SHH MB patients might benefit from the use of MYC inhibitors depleting aggressive SOX2$^+$ cells. Here, we use BET inhibitors to disrupt SHH signaling downstream of SMO. As BET activity is similarly needed to sustain MYC signaling in MB tissues (*53*), the efficacy displayed by BET inhibitors on depleting SOX2$^+$ cells might be due not only to their effect on GLI but also to that on MYC. Although our data suggest that GLI

signaling is activated in an MYC-dependent manner in MPC cultures, the mechanism by which a small subset of MYC-expressing SOX2$^+$ cells could be orchestrating MB relapse, as well as the roles that additional signaling mechanisms play, including Zic2, which was downregulated in SOX2$^+$ MB cells and shown to cooperate with GLI (*54*, *55*), and control neurogenesis of the GCPs (*56*) should be further explored.

In conclusion, here, we demonstrate the existence of a SOX2$^+$ cell reservoir with an astrocytic transcriptome that contributes to treatment resistance and cancer relapse. In these cells, SHH signaling is activated downstream of SMO. Thus, SMO inhibition causes the enrichment of residual MB tissues for SOX2$^+$ cells, which increases the chances of tumor relapse and dictates poor patient outcome. Conversely, inhibition of SHH signaling at the level of GLI depletes the vismodegib-resistant SOX2$^+$ reservoir and therefore improves patient outcome (Fig. 8I). Thus, inhibiting SHH signaling at the level of GLI has promising potential to improve survival in this challenging to treat MB patient population.

MATERIALS AND METHODS

Mouse studies

All mouse work was conducted in accordance with protocols approved by the Institutional Animal Care and Use Committee at the Medical University of South Carolina and the University of Miami. *Ptch1-LacZ* (*Ptch1^{1MPS}/J*), *Trp53* KO (*B6.129S2-Trp53^{tm1Tyj}/J*), *ND2:SmoA1* (*C57BL/6-Tg(Neurod2-Smo*A1)199Jols/J*), *Ptch1LoxP* (*B6;129T2-Ptch1tm1Bjw/WreyJ*), and *Gfap-Cre* (*FVB-Tg(GFAP-cre)25Mes/J*) strains were all obtained from the Jackson Laboratory and bred to generate the following colonies: *Ptch1-LacZ*, *Ptch1-LacZ; Trp53 KO*, *ND2:SmoA1*, and *Ptch1-Gfap*. Spontaneous tumors from *Ptch1-LacZ* (MB47: *Ptch1$^{+/-}$*) or *Ptch1-LacZ*; *Trp53* KO (MB1: *Ptch1$^{+/-}$; Trp53$^{+/-}$*) mice were expanded and maintained as allografts in 6- to 8-week-old *CD1-Foxn1^{nu}* (Charles River Laboratories).

For in vivo subcutaneous tumor treatments, 1×10^6 viable cells were implanted into the flanks of 6- to 8-week-old *CD1-Foxn1^{nu}* (*CD-1*) mice. Subcutaneous tumor volume was calculated using the formula (length × width^2)/2. For orthotopic allograft experiments, 1×10^5 viable cells were resuspended in 3 μl of Neurobasal-A serum-free media and implanted into the cerebella of 6- to 8-week-old *CD1* mice as before (*27*). Expansion and treatment of PDOX: RCMB18 (*57*), a courtesy of Dr. R. Wechsler-Reya (Sandford Burnham Prebys, La Jolla, CA), and SJSHHMB-14-7196 (SJSHHMB) (*58*), a courtesy of Dr. M. Roussel before publication (St. Jude Children Research Hospital, Memphis, TN), was performed by similarly orthotopically implanting 1×10^6 viable cells into the cerebella of 6- to 8-week-old *NSG* mice (*NOD.Cg-Prkdcscid Il2rgtm1Wjl/SzJ mice*). Two additional PDOX models, RCMB32, an SHH subtype from a Gorlin syndrome patient, and RCMB28, group 3 MB with an *MYC* amplification were also a courtesy of Wechsler-Reya (*59*) and used as controls for our immunohistochemistry (IHC) stainings.

All mice were dosed intraperitoneally and daily with indicated drugs: vismodegib (25 mg/kg), I-BET151 (30 mg/kg), JQ-1 (30 mg/kg), or BMS-986158 (3 mg/kg) dissolved in dimethyl sulfoxide to a final volume of 50 μl. Gant-61 was administrated subcutaneously every other day and dissolved in 50% ethanol and 50% corn oil. All compounds used for in vivo experiments were from Selleckchem, except BMS-986158, which was from BioVision.

For primary sphere formation and secondary tumor engraftment studies, mice harboring *Ptch1-LacZ* subcutaneous allografts (MB47) were treated for 8 days with vehicle, vismodegib (25 mg/kg), JQ-1 (30 mg/kg), or BMS-986158 (3 mg/kg). Residual tumors were harvested and then disaggregated mechanically and enzymatically using Accutase (Invitrogen) for 20 min. The viability of the resulting cell suspensions was evaluated by trypan blue exclusion (Invitrogen). For primary sphere formation evaluations, 3×10^3 viable cells/μl from residual MB tissues were resuspended in MPC media containing Neurobasal-A, GlutaMAX, B27, N2, epidermal growth factor (20 ng/ml), FGF (20 ng/ml), and penicillin-streptomycin (all from Invitrogen) (*22*), and the ability of these cells to form spheres ex vivo was determined 1 week later. For secondary tumor engraftment experiments, 1×10^5 viable cells obtained from similar residual tumors were resuspended in 3 μl of Neurobasal-A serum-free media and implanted into the cerebella of 6- to 8-week-old *CD1* mice as before (*27*). Symptom-free survival was used to determine implantation rate. Mice were sacrificed once they developed signs of brain tumor, including dome-shaped cranium indicative of hydrocephalus, tilted head, hunching, circling, loss of weight, or ataxia. The presence of brain tumors was confirmed by hematoxylin and eosin (H&E) staining. The tumor area was quantified in H&E-stained slides imaged on a Nikon Eclipse Ni or an Olympus IX7I microscope and measured using NIS or CellSens software, respectively. The number of positive cells in tumor tissues was assessed using a blinded visual score of stained tissues. Visual quantification was validated by processing images in ImageJ in batch mode via macro script. Particle size threshold was adjusted respectively, and automated particle count was performed as before (*60*).

Immunohistochemistry

After in vivo treatments, tumors were harvested and fixed for 48 hours in 10% formalin. Antigen retrieval on mouse-derived tissues or an MB tissue array (Biomax, BC17012c) was performed by steaming samples in citrate buffer for 30 min before staining for GLI2 (Aviva Systems Biology), GFAP, Ki67, SOX2 (Abcam), or cleaved caspase-3 (Cell Signaling Technology) according to the manufacturer's recommendations. For GLI1 (Invitrogen) IHC staining, samples were boiled in EDTA (pH 8.5) for 10 min instead. SOX2, GLI1, and GLI2 antibodies were validated using respective positive and negative tissues (fig. S1, A to C). Diaminobenzidine (DAB) reagent (DAKO) and a Vina Green chromogen kit (Biocare Medical) were applied for antigen detection. IHC stainings were counterstained with hematoxylin, except for double stainings using DAB and Vina Green reagents to detect nuclear proteins, in which no counterstaining was performed. DAB and Vina Green background staining for double IHC staining was determined after incubation of samples in the presence of the primary and secondary antibodies for one of the antigens and only the secondary for the other (fig. S1D). GLI1 and GLI2 staining in TMA was scored by a board-certified pathologist (K. G. Lindsey, Medical University of South Carolina, SC). For quantification of double-positive cells in TMA, slides were scanned on a Vectra Polaris instrument (PerkinElmer), and the resulting images were processed via Phenochart and analyzed using inForm software (Akoya Biosciences) as before (*61*). Quantifications were validated in a Nikon Eclipse Ni microscope.

Cell culture

MB tumors from *Ptch1-LacZ* (MB47) or *Ptch1-LacZ*; *Trp53 KO* (MB1, MB2) mice were enzymatically and mechanically digested using Accutase (Invitrogen), and the resulting cell suspensions were

maintained ex vivo in MPC media to generate vismodegib-resistant cultures, one *Ptch1-LacZ* with $Ptch1^{-/-}$ genotype (MPC-47) and two independent *Ptch1-LacZ*; *Trp53 KO* with $Ptch1^{-/-}$; $Trp53^{-/-}$ genotype (MPC-1 and MPC-2) cultures (*22*), or in Dulbecco's modified Eagle's medium (DMEM)/F12 (Gibco), B27, and penicillin-streptomycin to generate matching vismodegib-sensitive SHH-MB cultures (*28*, *29*). Similar cell culture media were used to expand *Ptch1-Gfap* tumors ex vivo. The isolation and culture of GCPs from P4-6 C57BL/6 mice was performed using a papain dissociation system (Worthington Biochemical Corporation). Cells were plated on poly-L-lysine (Millipore)–coated plates in Neurobasal-A, 1% GlutaMAX, 2% B27, penicillin-streptomycin, and KCl (250 mmol/liter) (*27*).

NIH-3T3 cells stably expressing a GLI-dependent firefly luciferase reporter gene and a constitutive Renilla luciferase reporter gene (Light2 cells) were maintained in DMEM with 10% fetal calf serum (FBS), G418 (0.2 μg/μl), and Zeocin (0.1 μg/μl). SHH signaling was induced in these cells by treating them with SAG (100 nM) in 0.1% FBS for 24 hours. GLI-driven firefly luciferase activity was normalized to the Renilla luciferase control, and its activity was determined using a dual luciferase kit (Promega) (*23*, *27*). Immortalized WT (*44*) and $Sufu^{-/-}$ (*45*) MEFs were cultured in DMEM and 10% FBS.

Cell and molecular biology

Cell viability was monitored by the reduction of 3-(4,5-dimethyl-2-thiazolyl) 2,5-diphenyl-2*H*-tetrazolium bromide (MTT) to formazan (*27*). Total RNA was TRIzol-extracted, and expression of the indicated genes was measured by quantitative real-time polymerase chain reaction (RT-qPCR) using TaqMan probes (Invitrogen) (*27*). RT-qPCR data were normalized to *GAPDH* reference gene. *Gli1* and *Ptch1* were used as SHH target genes. Because the lack of *Ptch1* expression, *Ptch2* was used as an SHH target gene in *Ptch1* mutant MB models as before (*22*, *23*, *27*). Radioimmuno-precipitation (RIPA buffer) assay buffer (Thermo Fisher Scientific) was used for protein extraction, and levels of the indicated proteins were determined by immunoblotting according to the manufacturer indications and using antibodies purchased from Cell Signaling Technology [GLI1, SOX2, MYC, HSP90, and glyceraldehyde-3-phosphate dehydrogenase (GAPDH)] or Aviva Systems Biology (GLI2) and listed in fig. S8. GAPDH was used as loading control. Chromatin immunoprecipitation analyses were performed by using the ChIP-IT Express Chromatin Immunoprecipitation Kit from Active Motif. Chromatin fragments were immunoprecipitated with BRD4 antibodies (Bethyl Laboratories) or immunoglobulin G (IgG) control. Relevant regions of the *Gli1* locus were amplified by qPCR using previously published probe sets (PS) and listed in fig. S8 (*62*). PS3 aligns 5′ to the transcription start site and, therefore, was used as a negative control. For flow cytometry analyses, cell suspensions were stained using a LIVE/DEAD viability kit (Invitrogen) and then incubated in Cytofix/Cytoperm solution (Becton Dickinson) before staining using corresponding fluorescent-conjugated antibody: SOX2-APC (BioLegend), GLI1-APC-Cy7, GLI2-FITC, and GFAP-PE (Novus Biologicals). Flow cytometry data were acquired using a LSRFortessa X-20 flow cytometer (Becton Dickinson) and analyzed using FlowJo software. Specificity of GLI1 and GLI2 antibodies for flow cytometry analyses was determined by comparing percentages of cells expressing GLI1 and GLI2 in vismodegib-sensitive SHH-MB cell cultures exposed to vehicle or vismodegib (fig. S2E). Two different sets of siRNA (siGENOME and siOnTarget) consisting of a pool of four sequences each were purchased from Dharmacon and used at 25 nM in 3×10^5 cells. Transfections were performed using Lipofectamine 2000 (Invitrogen). *GLI1*-expressing vector was a gift from the laboratory of Dr. D. Robbins, and *pCS2-MT GLI2 FL* (*GLI2)* was obtained from Addgene (plasmid #17648). Three small guide RNAs (sgRNAs) targeting the 5′ start site and two targeting the 3′ region of the coding domain (fig. S8) were selected for the CRISPR-Cas9–mediated silencing on *Myc* (fig. S8) using CHOPCHOP (https://chopchop.cbu.uib.no/) and cloned into a *lentiCRISPRv2* vector (Addgene, plasmid #104990). A total of 600 ng of each sgRNA (*sgMYC*) or 3 μg of the same vector containing a scramble sequence (*sgSC*) and 1 μg of *LentiCas9* vector (Addgene, plasmid #52962) were transfected into MPC cultures using Lipofectamine 2000. Four days later, cells were collected for further analyses. For cell proliferation assays, MPC cultures were plated in poly-L-lysine (Millipore)–coated glass chamber slides (Millipore) and incubated in the presence of bromodeoxyuridine (BrdU) (10 mM; Bio-Legend) for 2 hours before fixation with 16% paraformaldehyde and staining using anti-BrdU antibody (Cell Signaling Technology). Similar chamber slides were used to stain MPC cultures for cleaved caspase-3 (Cell Signaling Technology). All drugs used in our ex vivo experiments were purchased from Selleckchem, except BMS-986158, which was purchased from BioVision.

Imaging mass cytometry

All antibodies in the panel were initially tested by immunofluorescence and conjugated to metals using the Maxpar X8 Multimetal Labeling Kit (Fluidigm) according to the manufacturer's protocol. Data acquisition was performed on a Helios time-of-flight mass cytometer coupled to the Hyperion Imaging System (Fluidigm). Before laser ablation, optical images of slides were acquired using the Hyperion software. Laser ablation was performed at a resolution of approximately 1 mm and a frequency of 200 Hz.

scRNA-seq analyses

Previously generated scRNA-seq data from T.R.G's laboratory (University of North Carolina, Chapel Hill, NC) (*20*) were analyzed using R scripting. Cell populations were classified on the basis of an assignment of cell types to Louvain-Jaccard clusters and visualized by a *t*-distributed stochastic neighbor embedding (t-SNE) projection of the principal components analysis matrix as previously reported (*20*). Seurat toolkit (*63*) was used for the visualization of the gene expression levels in cells from vehicle- and vismodegib-treated tumors. Density plots represent the kernel density estimation of a gene expression or genes coexpression, improving the visualization of dropped-out genes (*64*). For the representation of coexpression with *Gli1* or *Gli2*, the sum of products was applied.

Gene expression profiling

R2 (http://r2.amc.nl) was used to analyze RNA-seq data from enhanced green fluorescent protein (eGFP)–$SOX2^+$ and $eGFP^-$ MB cells previously generated at the laboratory of Dr. P. Dirks (SickKids, Toronto, Canada) (*19*). For differential expression analyses, gene expression was transformed to $\log_2$, and SHH biomarkers contained in the Kyoto Encyclopedia of Genes and Genomes 48 genes Hedgehog Signaling Pathway (environmental information processing) elaborated at Kampen's laboratory (Amsterdam UMC, Amsterdam, The Netherlands) were used to filter genes. Expression was analyzed by performing a two-sided *t* test, and a false discovery rate test was applied for multiple testing correction.

Statistical analysis

Results from ex vivo experiments represent means ± SEM of at least three independent experiments. Analyses of stainings done in MPC cultures were performed by quantifying numbers of positive cells per field in at least five high-magnification fields per condition, from three independent experiments. For tumor size studies, the results shown represent the mean and SEM of tumor areas found in brain slides from at least four randomly assigned mice per experimental condition, and each dot in the graph represents an individual animal. For tissue IHC quantification, numbers of positive cells per field were quantified. The results shown represent mean and SEM of positive cells located in at least four random high-magnification fields from at least three different mice, where each dot in the graph represents an individual animal. The significance for two-group analyses was determined using an unpaired Student's *t* test. Multiple comparison analyses were performed using one-way analysis of variance (ANOVA), followed by a Dunnett post hoc. Kaplan-Meier methods were used to construct symptom-free survival curves using at least nine mice per experimental condition, and significance was evaluated using log-rank (Mantel-Cox) tests. Statistical significance (*) was reached when P value was <0.05.

SUPPLEMENTARY MATERIALS

Supplementary material for this article is available at https://science.org/doi/10.1126/sciadv.abj9138

View/request a protocol for this paper from *Bio-protocol*.

REFERENCES AND NOTES

1. D. N. Louis, A. Perry, G. Reifenberger, A. von Deimling, D. Figarella-Branger, W. K. Cavenee, H. Ohgaki, O. D. Wiestler, P. Kleihues, D. W. Ellison, The 2016 World Health Organization classification of tumors of the central nervous system: A summary. *Acta Neuropathol.* **131**, 803–820 (2016).
2. P. A. Northcott, A. Korshunov, H. Witt, T. Hielscher, C. G. Eberhart, S. Mack, E. Bouffet, S. C. Clifford, C. E. Hawkins, P. French, J. T. Rutka, S. Pfister, M. D. Taylor, Medulloblastoma comprises four distinct molecular variants. *J. Clin. Oncol.* **29**, 1408–1414 (2011).
3. R. J. Gilbertson, D. W. Ellison, The origins of medulloblastoma subtypes. *Annu. Rev. Pathol.* **3**, 341–365 (2008).
4. N. Dahmane, A. Ruiz i Altaba, Sonic hedgehog regulates the growth and patterning of the cerebellum. *Development* **126**, 3089–3100 (1999).
5. V. A. Wallace, Purkinje-cell-derived sonic hedgehog regulates granule neuron precursor cell proliferation in the developing mouse cerebellum. *Curr. Biol.* **9**, 445–448 (1999).
6. R. J. Wechsler-Reya, M. P. Scott, Control of neuronal precursor proliferation in the cerebellum by sonic hedgehog. *Neuron* **22**, 103–114 (1999).
7. C. Raffel, R. B. Jenkins, L. Frederick, D. Hebrink, B. Alderete, D. W. Fults, C. D. James, Sporadic medulloblastomas contain PTCH mutations. *Cancer Res.* **57**, 842–845 (1997).
8. Z.-J. Yang, T. Ellis, S. L. Markant, T.-A. Read, J. D. Kessler, M. Bourboulas, U. Schüller, R. Machold, G. Fishell, D. H. Rowitch, B. J. Wainwright, R. J. Wechsler-Reya, Medulloblastoma can be initiated by deletion of patched in lineage-restricted progenitors or stem cells. *Cancer Cell* **14**, 135–145 (2008).
9. J. Svard, B. Rozell, R. Toftgard, S. Teglund, Tumor suppressor gene co-operativity in compound patched1 and suppressor of fused heterozygous mutant mice. *Mol. Carcinog.* **48**, 408–419 (2009).
10. A. Ruiz i Altaba, Hedgehog signaling and the Gli code in stem cells, cancer, and metastases. *Sci. Signal.* **4**, pt9 (2011).
11. D. J. Robbins, D. L. Fei, N. A. Riobo, The Hedgehog signal transduction network. *Sci. Signal.* **5**, re6 (2012).
12. B. Stecca, A. Ruiz i Altaba, Context-dependent regulation of the GLI code in cancer by HEDGEHOG and non-HEDGEHOG signals. *J. Mol. Cell Biol.* **2**, 84–95 (2010).
13. Y. Li, Q. Song, B. W. Day, Phase I and phase II sonidegib and vismodegib clinical trials for the treatment of paediatric and adult MB patients: A systemic review and meta-analysis. *Acta Neuropathol. Commun.* **7**, 123 (2019).
14. C. M. Rudin, C. L. Hann, J. Laterra, R. L. Yauch, C. A. Callahan, L. Fu, T. Holcomb, J. Stinson, S. E. Gould, B. Coleman, P. M. L. Russo, D. D. Von Hoff, F. J. de Sauvage, J. A. Low, Treatment of medulloblastoma with hedgehog pathway inhibitor GDC-0449. *N. Engl. J. Med.* **361**, 1173–1178 (2009).
15. G. J. P. Dijkgraaf, B. Alicke, L. Weinmann, T. Januario, K. West, Z. Modrusan, D. Burdick, R. Goldsmith, K. Robarge, D. Sutherlin, S. J. Scales, S. E. Gould, R. L. Yauch, F. J. de Sauvage, Small molecule inhibition of GDC-0449 refractory smoothened mutants and downstream mechanisms of drug resistance. *Cancer Res.* **71**, 435–444 (2011).
16. S. Pricl, B. Cortelazzi, V. D. Col, D. Marson, E. Laurini, M. Fermeglia, L. Licitra, S. Pilotti, P. Bossi, F. Perrone, Smoothened (SMO) receptor mutations dictate resistance to vismodegib in basal cell carcinoma. *Mol. Oncol.* **9**, 389–397 (2015).
17. H. J. Sharpe, G. Pau, G. J. Dijkgraaf, N. Basset-Seguin, Z. Modrusan, T. Januario, V. Tsui, A. B. Durham, A. A. Dlugosz, P. M. Haverty, R. Bourgon, J. Y. Tang, K. Y. Sarin, L. Dirix, D. C. Fisher, C. M. Rudin, H. Sofen, M. R. Migden, R. L. Yauch, F. J. de Sauvage, Genomic analysis of smoothened inhibitor resistance in basal cell carcinoma. *Cancer Cell* **27**, 327–341 (2015).
18. H. J. Selvadurai, E. Luis, K. Desai, X. Lan, M. C. Vladoiu, O. Whitley, C. Galvin, R. J. Vanner, L. Lee, H. Whetstone, M. Kushida, T. Nowakowski, P. Diamandis, C. Hawkins, G. Bader, A. Kriegstein, M. D. Taylor, P. B. Dirks, Medulloblastoma arises from the persistence of a rare and transient $Sox2^+$ granule neuron precursor. *Cell Rep.* **31**, 107511 (2020).
19. R. J. Vanner, M. Remke, M. Gallo, H. J. Selvadurai, F. Coutinho, L. Lee, M. Kushida, R. Head, S. Morrissy, X. Zhu, T. Aviv, V. Voisin, I. D. Clarke, Y. Li, A. J. Mungall, R. A. Moore, Y. Ma, S. J. M. Jones, M. A. Marra, D. Malkin, P. A. Northcott, M. Kool, S. M. Pfister, G. Bader, K. Hochedlinger, A. Korshunov, M. D. Taylor, P. B. Dirks, Quiescent $Sox2^+$ cells drive hierarchical growth and relapse in sonic hedgehog subgroup medulloblastoma. *Cancer Cell* **26**, 33–47 (2014).
20. J. K. Ocasio, B. Babcock, D. Malawsky, S. J. Weir, L. Loo, J. M. Simon, M. J. Zylka, D. Hwang, T. Dismuke, M. Sokolsky, E. P. Rosen, R. Vibhakar, J. Zhang, O. Saulnier, M. Vladoiu, I. El-Hamamy, L. D. Stein, M. D. Taylor, K. S. Smith, P. A. Northcott, A. Colaneri, K. Wilhelmsen, T. R. Gershon, scRNA-seq in medulloblastoma shows cellular heterogeneity and lineage expansion support resistance to SHH inhibitor therapy. *Nat. Commun.* **10**, 5829 (2019).
21. S. Zhang, X. Xiong, Y. Sun, Functional characterization of SOX2 as an anticancer target. *Signal Transduct. Target. Ther.* **5**, 135 (2020).
22. J. Rodriguez-Blanco, L. Pednekar, C. Penas, B. Li, V. Martin, J. Long, E. Lee, W. A. Weiss, C. Rodriguez, N. Mehrdad, D. M. Nguyen, N. G. Ayad, P. Rai, A. J. Capobianco, D. J. Robbins, Inhibition of WNT signaling attenuates self-renewal of SHH-subgroup medulloblastoma. *Oncogene* **36**, 6306–6314 (2017).
23. J. Long, B. Li, J. Rodriguez-Blanco, C. Pastori, C.-H. Volmar, C. Wahlestedt, A. Capobianco, F. Bai, X.-H. Pei, N. G. Ayad, D. J. Robbins, The BET bromodomain inhibitor I-BET151 acts downstream of smoothened protein to abrogate the growth of hedgehog protein-driven cancers. *J. Biol. Chem.* **289**, 35494–35502 (2014).
24. Y. Tang, S. Gholamin, S. Schubert, M. I. Willardson, A. Lee, P. Bandopadhayay, G. Bergthold, S. Masoud, B. Nguyen, N. Vue, B. Balansay, F. Yu, S. Oh, P. Woo, S. Chen, A. Ponnuswami, M. Monje, S. X. Atwood, R. J. Whitson, S. Mitra, S. H. Cheshier, J. Qi, R. Beroukhim, J. Y. Tang, R. Wechsler-Reya, A. E. Oro, B. A. Link, J. E. Bradner, Y.-J. Cho, Epigenetic targeting of hedgehog pathway transcriptional output through BET bromodomain inhibition. *Nat. Med.* **20**, 732–740 (2014).
25. A. Alvarez-Trotta, Z. Wang, E. Shersher, B. Li, J. Long, I. Lohse, C. Wahlestedt, W. El-Rifai, D. J. Robbins, A. J. Capobianco, The bromodomain inhibitor IBET-151 attenuates vismodegib-resistant esophageal adenocarcinoma growth through reduction of GLI signaling. *Oncotarget* **11**, 3174–3187 (2020).
26. M. Lauth, A. Bergstrom, T. Shimokawa, R. Toftgard, Inhibition of GLI-mediated transcription and tumor cell growth by small-molecule antagonists. *Proc. Natl. Acad. Sci. U.S.A.* **104**, 8455–8460 (2007).
27. J. Rodriguez-Blanco, B. Li, J. Long, C. Shen, F. Yang, D. Orton, S. Collins, N. Kasahara, N. G. Ayad, H. J. McCrea, M. F. Roussel, W. A. Weiss, A. J. Capobianco, D. J. Robbins, A CK1α activator penetrates the brain and shows efficacy against drug-resistant metastatic medulloblastoma. *Clin. Cancer Res.* **25**, 1379–1388 (2019).
28. X. Zhao, T. Ponomaryov, K. J. Ornell, P. Zhou, S. K. Dabral, E. Pak, W. Li, S. X. Atwood, R. J. Whitson, A. L. S. Chang, J. Li, A. E. Oro, J. A. Chan, J. F. Kelleher, R. A. Segal, RAS/MAPK activation drives resistance to smo inhibition, metastasis, and tumor evolution in shh pathway-dependent tumors. *Cancer Res.* **75**, 3623–3635 (2015).
29. C. Penas, M. E. Maloof, V. Stathias, J. Long, S. K. Tan, J. Mier, Y. Fang, C. Valdes, J. Rodriguez-Blanco, C.-M. Chiang, D. J. Robbins, D. J. Liebl, J. K. Lee, M. E. Hatten, J. Clarke, N. G. Ayad, Time series modeling of cell cycle exit identifies Brd4 dependent regulation of cerebellar neurogenesis. *Nat. Commun.* **10**, 3028 (2019).
30. Y. Xu, C. R. Vakoc, Targeting cancer cells with BET bromodomain inhibitors. *Cold Spring Harb. Perspect. Med.* **7**, a026674 (2017).
31. M. M. Mita, A. C. Mita, Bromodomain inhibitors a decade later: A promise unfulfilled? *Br. J. Cancer* **123**, 1713–1714 (2020).
32. T. Shorstova, W. D. Foulkes, M. Witcher, Achieving clinical success with BET inhibitors as anti-cancer agents. *Br J. Cancer* **124**, 1478–1490 (2021).
33. B. Stecca, A. Ruiz i Altaba, A GLI1-p53 inhibitory loop controls neural stem cell and tumour cell numbers. *EMBO J.* **28**, 663–676 (2009).
34. J. W. Yoon, M. Lamm, S. Iannaccone, N. Higashiyama, K. F. Leong, P. Iannaccone, D. Walterhouse, p53 modulates the activity of the GLI1 oncogene through interactions with the shared coactivator TAF9. *DNA Repair* **34**, 9–17 (2015).

35. J. W. Yoon, M. Gallant, M. L. G. Lamm, S. Iannaccone, K.-F. Vieux, M. Proytcheva, E. Hyjek, P. Iannaccone, D. Walterhouse, Noncanonical regulation of the hedgehog mediator GLI1 by c-MYC in Burkitt lymphoma. *Mol. Cancer Res.* **11**, 604–615 (2013).
36. F. Varnat, I. Siegl-Cachedenier, M. Malerba, P. Gervaz, A. Ruiz i Altaba, Loss of WNT-TCF addiction and enhancement of HH-GLI1 signalling define the metastatic transition of human colon carcinomas. *EMBO Mol. Med.* **2**, 440–457 (2010).
37. M. J. Huang, Y. C. Cheng, C. R. Liu, S. Lin, H. E. Liu, A small-molecule c-Myc inhibitor, 10058-F4, induces cell-cycle arrest, apoptosis, and myeloid differentiation of human acute myeloid leukemia. *Exp. Hematol.* **34**, 1480–1489 (2006).
38. C.-P. Lin, J.-D. Liu, J.-M. Chow, C.-R. Liu, H. E. Liu, Small-molecule c-Myc inhibitor, 10058-F4, inhibits proliferation, downregulates human telomerase reverse transcriptase and enhances chemosensitivity in human hepatocellular carcinoma cells. *Anticancer Drugs* **18**, 161–170 (2007).
39. M. Sayyadi, A. Safaroghli-Azar, M. Safa, H. Abolghasemi, M. Momeny, D. Bashash, NF-κB-dependent mechanism of action of c-Myc inhibitor 10058-F4: Highlighting a promising effect of c-Myc inhibition in leukemia cells, irrespective of p53 status. *Iran J. Pharm. Res.* **19**, 153–165 (2020).
40. C. Pastori, M. Daniel, C. Penas, C.-H. Volmar, A. L. Johnstone, S. P. Brothers, R. M. Graham, B. Allen, J. N. Sarkaria, R. J. Komotar, C. Wahlestedt, N. G. Ayad, BET bromodomain proteins are required for glioblastoma cell proliferation. *Epigenetics* **9**, 611–620 (2014).
41. S. Tanigawa, M. Fujita, C. Moyama, S. Ando, H. Ii, Y. Kojima, T. Fujishita, M. Aoki, H. Takeuchi, T. Yamanaka, Y. Takahashi, N. Hashimoto, S. Nakata, Inhibition of Gli2 suppresses tumorigenicity in glioblastoma stem cells derived from a de novo murine brain cancer model. *Cancer Gene Ther.* **28**, 1339–1352 (2021).
42. F. Spriano, A. Stathis, F. Bertoni, Targeting BET bromodomain proteins in cancer: The example of lymphomas. *Pharmacol. Ther.* **215**, 107631 (2020).
43. F. Li, K. R. MacKenzie, P. Jain, C. Santini, D. W. Young, M. M. Matzuk, Metabolism of JQ1, an inhibitor of bromodomain and extra terminal bromodomain proteins, in human and mouse liver microsomes†. *Biol. Reprod.* **103**, 427–436 (2020).
44. R. J. Lipinski, M. F. Bijlsma, J. J. Gipp, D. J. Podhaizer, W. Bushman, Establishment and characterization of immortalized Gli-null mouse embryonic fibroblast cell lines. *BMC Cell Biol.* **9**, 49 (2008).
45. J. Svärd, K. Heby-Henricson, M. Persson-Lek, B. Rozell, M. Lauth, A. Bergström, J. Ericson, R. Toftgård, S. Teglund, Genetic elimination of suppressor of fused reveals an essential repressor function in the mammalian hedgehog signaling pathway. *Dev. Cell* **10**, 187–197 (2006).
46. G. W. Robinson, B. A. Orr, G. Wu, S. Gururangan, T. Lin, I. Qaddoumi, R. J. Packer, S. Goldman, M. D. Prados, A. Desjardins, M. Chintagumpala, N. Takebe, S. C. Kaste, M. Rusch, S. J. Allen, A. Onar-Thomas, C. F. Stewart, M. Fouladi, J. M. Boyett, R. J. Gilbertson, T. Curran, D. W. Ellison, A. Gajjar, Vismodegib exerts targeted efficacy against recurrent sonic hedgehog-subgroup medulloblastoma: Results from phase II pediatric brain tumor consortium studies PBTC-025B and PBTC-032. *J. Clin. Oncol.* **33**, 2646–2654 (2015).
47. F. M. G. Cavalli, M. Remke, L. Rampasek, J. Peacock, D. J. H. Shih, B. Luu, L. Garzia, J. Torchia, C. Nor, A. S. Morrissy, S. Agnihotri, Y. Y. Thompson, C. M. Kuzan-Fischer, H. Farooq, K. Isaev, C. Daniels, B.-K. Cho, S.-K. Kim, K.-C. Wang, J. Y. Lee, W. A. Grajkowska, M. Perek-Polnik, A. Vasiljevic, C. Faure-Conter, A. Jouvet, C. Giannini, A. A. N. Rao, K. K. W. Li, H.-K. Ng, C. G. Eberhart, I. F. Pollack, R. L. Hamilton, G. Y. Gillespie, J. M. Olson, S. Leary, W. A. Weiss, B. Lach, L. B. Chambless, R. C. Thompson, M. K. Cooper, R. Vibhakar, P. Hauser, M.-L. C. van Veelen, J. M. Kros, P. J. French, Y. S. Ra, T. Kumabe, E. López-Aguilar, K. Zitterbart, J. Sterba, G. Finocchiaro, M. Massimino, E. G. V. Meir, S. Osuka, T. Shofuda, A. Klekner, M. Zollo, J. R. Leonard, J. B. Rubin, N. Jabado, S. Albrecht, J. Mora, T. E. V. Meter, S. Jung, A. S. Moore, A. R. Hallahan, J. A. Chan, D. P. C. Tirapelli, C. G. Carlotti, M. Fouladi, J. Pimentel, C. C. Faria, A. G. Saad, L. Massimi, L. M. Liau, H. Wheeler, H. Nakamura, S. K. Elbabaa, M. Perezpeña-Diazconti, F. C. P. de León, S. Robinson, M. Zapotocky, A. Lassaletta, A. Huang, C. E. Hawkins, U. Tabori, E. Bouffet, U. Bartels, P. B. Dirks, J. T. Rutka, G. D. Bader, J. Reimand, A. Goldenberg, V. Ramaswamy, M. D. Taylor, Intertumoral heterogeneity within medulloblastoma subgroups. *Cancer Cell* **31**, 737–754.e6 (2017).
48. A. D. Berezovsky, L. M. Poisson, D. Cherba, C. P. Webb, A. D. Transou, N. W. Lemke, X. Hong, L. A. Hasselbach, S. M. Irtenkauf, T. Mikkelsen, A. C. de Carvalho, Sox2 promotes malignancy in glioblastoma by regulating plasticity and astrocytic differentiation. *Neoplasia* **16**, 193–206, 206.e19–e25 (2014).
49. R. Tao, N. Murad, Z. Xu, P. Zhang, K. Okonechnikov, M. Kool, S. Rivero-Hinojosa, C. Lazarski, P. Zheng, Y. Liu, C. G. Eberhart, B. R. Rood, R. Packer, Y. Pei, MYC drives group 3 medulloblastoma through transformation of $Sox2^+$ astrocyte progenitor cells. *Cancer Res.* **79**, 1967–1980 (2019).
50. M. Yao, P. B. Ventura, Y. Jiang, F. J. Rodriguez, L. Wang, J. S. A. Perry, Y. Yang, K. Wahl, R. B. Crittenden, M. L. Bennett, L. Qi, C.-C. Gong, X.-N. Li, B. A. Barres, T. P. Bender, K. S. Ravichandran, K. A. Janes, C. G. Eberhart, H. Zong, Astrocytic trans-differentiation completes a multicellular paracrine feedback loop required for medulloblastoma tumor growth. *Cell* **180**, 502–520.e19 (2020).
51. M. P. Fogarty, B. A. Emmenegger, L. L. Grasfeder, T. G. Oliver, R. J. Wechsler-Reya, Fibroblast growth factor blocks sonic hedgehog signaling in neuronal precursors and tumor cells. *Proc. Natl. Acad. Sci. U.S.A.* **104**, 2973–2978 (2007).
52. J. Lu, M. Chen, X.-R. Ren, J. Wang, H. K. Lyerly, L. Barak, W. Chen, Regulation of hedgehog signaling by Myc-interacting zinc finger protein 1, Miz1. *PLOS ONE* **8**, e63353 (2013).
53. P. Bandopadhayay, G. Bergthold, B. Nguyen, S. Schubert, S. Gholamin, Y. Tang, S. Bolin, S. E. Schumacher, R. Zeid, S. Masoud, F. Yu, N. Vue, W. J. Gibson, B. R. Paolella, S. Mitra, S. Cheshier, J. Qi, K.-W. Liu, R. Wechsler-Reya, W. A. Weiss, F. J. Swartling, M. W. Kieran, J. E. Bradner, R. Beroukhim, Y.-J. Cho, BET bromodomain inhibition of MYC-amplified medulloblastoma. *Clin. Cancer Res.* **20**, 912–925 (2014).
54. R. Brewster, J. Lee, A. Ruiz i Altaba, Gli/Zic factors pattern the neural plate by defining domains of cell differentiation. *Nature* **393**, 579–583 (1998).
55. Y. Koyabu, K. Nakata, K. Mizugishi, J. Aruga, K. Mikoshiba, Physical and functional interactions between Zic and Gli proteins. *J. Biol. Chem.* **276**, 6889–6892 (2001).
56. J. Aruga, N. Yokota, M. Hashimoto, T. Furuichi, M. Fukuda, K. Mikoshiba, A novel zinc finger protein, zic, is involved in neurogenesis, especially in the cell lineage of cerebellar granule cells. *J. Neurochem.* **63**, 1880–1890 (1994).
57. S. N. Brun, S. L. Markant, L. A. Esparza, G. Garcia, D. Terry, J.-M. Huang, M. S. Pavlyukov, X.-N. Li, G. A. Grant, J. R. Crawford, M. L. Levy, E. M. Conway, L. H. Smith, I. Nakano, A. Berezov, M. I. Greene, Q. Wang, R. J. Wechsler-Reya, Survivin as a therapeutic target in Sonic hedgehog-driven medulloblastoma. *Oncogene* **34**, 3770–3779 (2015).
58. K. S. Smith, K. Xu, K. S. Mercer, F. Boop, P. Klimo, M. DeCupyere, J. Grenet, S. Robinson, P. Dunphy, S. J. Baker, D. W. Ellison, T. E. Merchant, S. A. Upadayaya, A. Gajjar, G. Wu, B. A. Orr, G. W. Robinson, P. A. Northcott, M. F. Roussel, Patient-derived orthotopic xenografts of pediatric brain tumors: A St. Jude resource. *Acta Neuropathol.* **140**, 209–225 (2020).
59. Y. Pei, K.-W. Liu, J. Wang, A. Garancher, R. Tao, L. A. Esparza, D. L. Maier, Y. T. Udaka, N. Murad, S. Morrissy, H. Seker-Cin, S. Brabetz, L. Qi, M. Kogiso, S. Schubert, J. M. Olson, Y.-J. Cho, X.-N. Li, J. R. Crawford, M. L. Levy, M. Kool, S. M. Pfister, M. D. Taylor, R. J. Wechsler-Reya, HDAC and PI3K antagonists cooperate to inhibit growth of MYC-driven medulloblastoma. *Cancer Cell* **29**, 311–323 (2016).
60. E. C. Jensen, Quantitative analysis of histological staining and fluorescence using ImageJ. *Anat. Rec.* **296**, 378–381 (2013).
61. H. Mori, J. Bolen, L. Schuetter, P. Massion, C. C. Hoyt, S. V. Berg, L. Esserman, A. D. Borowsky, M. J. Campbell, Characterizing the tumor immune microenvironment with tyramide-based multiplex immunofluorescence. *J. Mammary Gland Biol. Neoplasia* **25**, 417–432 (2020).
62. R. Taylor, J. Long, J. W. Yoon, R. Childs, K. B. Sylvestersen, M. L. Nielsen, K.-F. Leong, S. Iannaccone, D. O. Walterhouse, D. J. Robbins, P. Iannaccone, Regulation of GLI1 by cis DNA elements and epigenetic marks. *DNA Repair* **79**, 10–21 (2019).
63. A. Butler, P. Hoffman, P. Smibert, E. Papalexi, R. Satija, Integrating single-cell transcriptomic data across different conditions, technologies, and species. *Nat. Biotechnol.* **36**, 411–420 (2018).
64. J. Alquicira-Hernandez, J. E. Powell, Nebulosa recovers single cell gene expression signals by kernel density estimation. *Bioinformatics* **37**, 2485–2487 (2021).

Acknowledgments: I thank my postdoctoral mentor, Dr. D. Robbins, for training during the years spent in his laboratory and for providing advice during the completion of this manuscript. We also thank Dr. D. Guttridge, Dr. D. Wang, Dr. M. Roussel, Dr. W. Weiss, Dr. R. Wechsler-Reya, and Dr. M. Taylor for providing insights during discussions regarding this manuscript. We would also like to thank the Translational Science Shared Resource at Hollings Cancer Center (supported by a P30 CA138313) for their work on tissue processing. Schematics were created using BioRender.com. **Funding:** This work was supported by the American Cancer Society Institutional Research Grant awarded to the Hollings Cancer Center: IRG-19-137-20 (to J.R.-B.), the Rally Foundation Career Development Award: 20CDN46 (to J.R.-B.), the National Institute of Neurological Disorders and Stroke of the National Institutes of Health Award K01NS119351 (to J.R.-B.), and SCTR grant UL1TR001450 (to J.R.-B.). **Author contributions:** Conceptualization: J.R.-B. and H.J.M. Methodology/investigation/visualization: M.S.-S., A.O., A.D.S., S.M.G., O.S., C.Se., C. Sh., C.K., J.R.-B., F.Y., D.T.W., and K.G.L. Animal studies: M.S.-S. and J.R.-B. Bioinformatic analyses: J.M.P., B.R.B., A.S.-M., T.R.G., and J.R.-B. Supervision: J.R.-B. Writing: J.R.-B., H.J.M., V.M., and J.M.P. **Competing interests**: The authors declare that they have no competing interests. **Data and materials availability**: All data needed to evaluate the conclusions in the paper are present in the paper and/or the Supplementary Materials. Such data, code, and materials are available to any researcher. PDOX tissues could be provided by Roussel (SJSHHMB-14-7196) or Wechsler-Reya (RCMB18, RCMB28, and RCM32) pending scientific review and a completed material transfer agreement. Requests for these tissues should be submitted to these investigators. GSE48766 (Dirks) and GSE129730 (T.R.G.) datasets were used in this manuscript.

Submitted 9 June 2021
Accepted 3 June 2022
Published 20 July 2022
10.1126/sciadv.abj9138

ScienceAdvances

Noncanonical activation of GLI signaling in SOX2+ cells drives medulloblastoma relapse

Marzena Swiderska-Syn, Jlia Mir-Pedrol, Alexander Oles, Olga Schleuger, April D. Salvador, Sean M. Greiner, Cara Seward, Fan Yang, Benjamin R. Babcock, Chen Shen, Daniel T. Wynn, Avencia Sanchez-Mejias, Timothy R. Gershon, Vanesa Martin, Heather J. McCrea, Kathryn G. Lindsey, Carsten Krieg, and Jezabel Rodriguez-Blanco

Sci. Adv., **8** (29), eabj9138.
DOI: 10.1126/sciadv.abj9138